



# Bulletin of the Mineral Research and Exploration

<http://bulletin.mta.gov.tr>

BULLETIN OF THE MINERAL RESEARCH AND EXPLORATION	
CONTENTS	
Geological, mineralogical and geochemical properties of the Dağbaşı skarn ores (Araklı-Trabzon, NE Turkey)	165-194
...	...

## Geological, mineralogical and geochemical properties of the Dağbaşı skarn ores (Araklı-Trabzon, NE Turkey)

Yılmaz DEMİR<sup>a\*</sup>

<sup>a</sup> Recep Tayyip Erdoğan University, Department of Geological Engineering, 53100 Rize/Turkey orcid.org 0000-0001-6608-4823

Research Article

### Keywords:

Dağbaşı skarn ore, skarn mineralogy, skarn geochemistry, Dağbaşı granitoid, Araklı-Trabzon.

### ABSTRACT

The Dağbaşı skarns have developed as an exoskarn type along the nearest border of Upper Cretaceous Dağbaşı Granitoid and block- and lens-shaped limestones of Berdiga formation located in the Liassic volcanics. The early garnets are predominantly grossular type ( $\text{And}_{0-0.81}\text{Grs}_{59.69-78.65}\text{Prs}_{21.35-38.11}$ ), while pyroxenes have a composition between diopside and hedenbergite ( $\text{Hed}_{24.44-31.81}\text{Diy}_{67.3-76.99}\text{Joh}_{0.52-0.88}$ ). The late garnets are characterized by high andradite ( $\text{And}_{74.67-100}\text{Grs}_{0-22.8}\text{Prs}_{0-4.51}$ ), and late pyroxenes by increasing johannsenite content ( $\text{Hed}_{22.17-62.63}\text{Diy}_{0-36.2}\text{Joh}_{31.86-76.69}$ ). High andradite content of late garnets is similar to Cu-Fe-type skarns, whereas the higher johannsenite and Mn/Fe ratios of pyroxenes are similar to Zn-type skarns. Higher andraditic garnets indicate an oxidized-type skarn and association with the shallow emplacement of intrusion. Increasing And/Gr ratios of garnets, from core to rim, also point out to increasing degree of oxidation. The retrograde skarn minerals are epidote, tremolite-actinolite, quartz, calcite, and chlorite. The ore minerals are composed of magnetite, hematite, pyrrhotite, pyrite, chalcopyrite, sphalerite, and galena. The Ag content of the galena (1.18-1.43wt%) suggests significant silver potential. Dağbaşı Granitoid shows high-K (2.38-3.75wt.%  $\text{K}_2\text{O}$ ), calc-alkaline, metaluminous-peraluminous transitional ( $\text{A/CNK}=0.88-1.23$ ) and volcanic arc type granitoid. The various main and trace element contents of the granodiorite observed along the skarn zones show similarities with Fe-Cu-Zn type skarn-related granitoids, whereas there is no clear relation between the skarn type and composition of other granitoids. Therefore, the presence of sulfur phases, in addition to the oxide ore suggests that geochemical characteristics of granitoid had a large effect on the mineral composition.

Received Date: 09.01.2018

Accepted Date: 25.05.2018

## 1. Introduction

The northeast Black Sea Region is an important metallogenic province of Turkey containing different types of ore deposits. In addition to the predominantly observed massive sulfide-type deposits, hydrothermal, skarn, and porphyry deposits are the other main types of ore mineralizations in the region. The region contain a large number of skarn-type ore deposits, due to the widespread outcrop of carbonate rocks (Berdiga formation) and granitic intrusions which cut these carbonate rocks. Çambaşı, Kotana, Kirazören, Ögene, Özdil, Dağbaşı, Kartiba, Sivrikaya, Demirköy, Eğrikar, Camiboğazı, and Arnastal are some of these

well-known skarn occurrences (Demir et al., 2017) (Figure 1).

Some studies performed on the skarn-type deposits of the region (Aslan, 1991; Hasançebi, 1993; Saraç, 2003; Çiftçi and Vıçıl, 2003; Çiftçi, 2011; Sipahi, 2011; Kurt, 2014; Sipahi et al., 2017; Demir et al., 2017) have demonstrated that these deposits show many differences in terms of ore types, alteration products, and formation conditions. According to these studies, while exoskarn-type mineralization has been reported from Özdil, Kartiba, Sivrikaya, Çambaşı, Kotana, Arnastal, and Camiboğazı deposits, both endoskarn- and exoskarn-type deposits have been

\* Corresponding author: Yılmaz DEMİR, [yilmaz.demir@erdogan.edu.tr](mailto:yilmaz.demir@erdogan.edu.tr)  
<http://dx.doi.org/10.19111/bulletinofmre.457070>

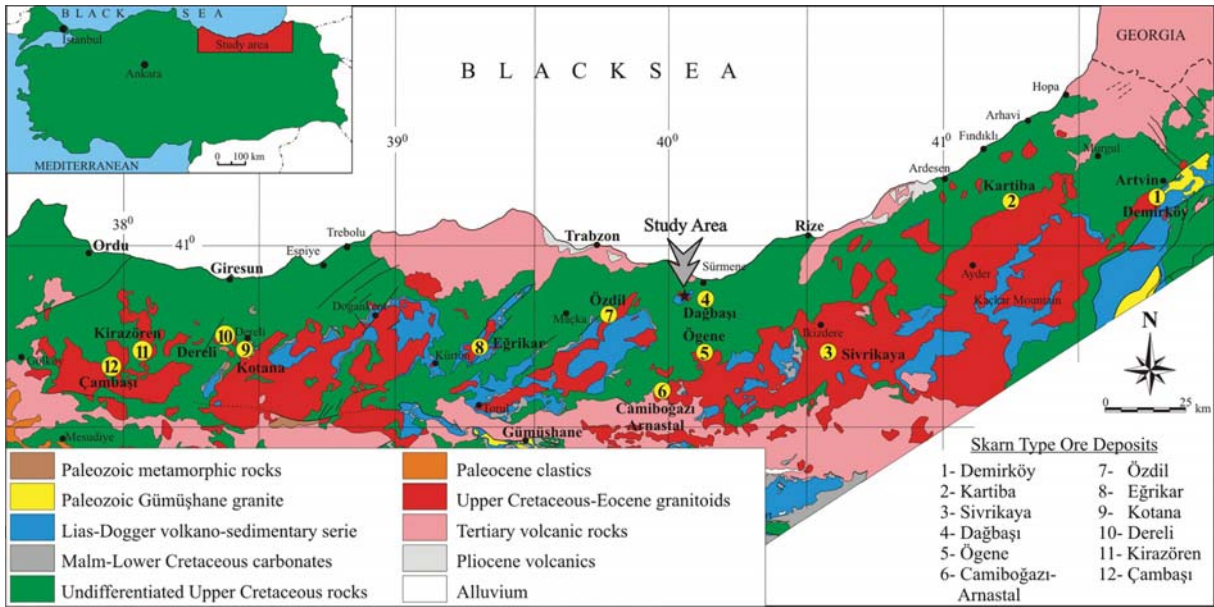


Figure 1- Geological map of the Eastern Black Sea Region and distribution of some skarn type deposits (Modified after Güven et al., 1998).

reported from Kirazören, Ögene, and Eğrikar deposits. Ore in the Özdil, Kartiba, Camiboğazı, and Sivrikaya deposits consists of oxide minerals (magnetite and hematite) while sulfur minerals accompany oxide phases in the Arnastal, Kotana, Kirazören, Eğrikar, and Dağbaşı deposits (Demir et al., 2017). In terms of host rocks, the age of carbonates ranges from Early Jurassic to Late Cretaceous and the age of intrusions from Jurassic to Eocene (Sipahi et al., 2017; Demir et al., 2017). In spite of these studies, it is understood that skarn-type deposits are less well investigated in comparison with the other types of deposits in the region, so the geological, mineralogical, and geochemical differences between these deposits have not been sufficiently clarified.

Dağbaşı skarn ores, the subject of this study, have been studied by Gülibrahimoğlu (1986) and Hasançebi (1993). In these studies, the presence of magnetite, specularite, pyrite, chalcopyrite, and sphalerite has been reported, but the skarn mineralogy has not been investigated. Granitic rocks in the region which played an important role in the skarn developments have been studied by Kaygusuz (1992), Aydınçakır (2006), and Kaygusuz and Aydınçakır (2011). They reported that these granites are I-type with low to medium K content and show properties of volcanic-arc-type calc-alkaline granitoids. They also reported that fractional crystallization and magma mixing were the main processes for these granite occurrences.

Skarn-type deposits occur as a result of the metasomatic process between granitoid and carbonate host rocks. At the early stage of this process, prograde skarn minerals develop due to the high temperature of intruding granites, whereas retrograde skarn minerals develop at the late stage with decreasing temperatures. Previous studies have shown that the anhydrous silicate minerals (such as garnet and pyroxene) develop in the prograde stage while the hydrous silicate minerals (such as epidote, amphibole, and chlorite) develop in the retrograde stage (Einaudi et al., 1981; Meinert, 1992; Orhan and Mutlu, 2009; Oyman, 2010).

Previous researchers showed a relationship between the garnet, pyroxene composition, and metal content of the skarn and the oxidation degree, and the classification was made accordingly (Einaudi et al., 1981; Einaudi and Burt, 1982; Nakona et al., 1994; Nakona, 1998; Meinert et al., 2005). In this classification, pyroxenes with high Mn content (johannsenite) correspond to the Zn-type skarns, while pyroxenes ranging between diopside and hedenbergite compositions correspond to the Cu-Fe-type skarns. According to these studies, oxidized skarns have high andradite and low spessartine and almandine contents. Some other studies have also shown that the increasing And/Grs ratios, from core to rim, reflect increasing oxidation degree in the zoned garnet crystals (Collins, 1977; Newberry, 1983; Abu el Enen et al., 2004). Newberry (1991) pointed out that in the reduced skarns, pyroxene is more commonly observed than

garnet and has a hedenbergite composition, whereas in the oxidized skarns pyroxene is less commonly observed and has a composition between diopside and hedenbergite.

The relationships between chemical compositions of granitoids and skarn types and their metal contents have been investigated by many researchers (Kwak and White, 1982; Newberry and Swanson, 1986; Meinert, 1995; Meinert et al., 2005). In these studies, it was shown that skarn-related granitoids are mostly associated with normal calc-alkaline intrusions, W, Sn, and Mo skarns are associated with intra-continental granitoids, and Fe, Cu, Zn, and Au containing skarns are associated with I-type island arc granitoids. With respect to the Al saturation, Sn skarns are associated with peraluminous plutons which develop as a result of melting of sedimentary rocks of continental crust. On the other hand, calcic Fe skarns are associated with metaluminous island arc plutons and other types of skarns are associated with granitoids of metaluminous–peraluminous transitions.

In this study, four different skarn locations have been defined around the Dağbaşı area. The geological and mineralogical properties of these skarn zones have been studied by systematic sampling. Garnet and pyroxene compositions have been studied in detail, because they give critical information on the classification of skarn deposits, developments of formation conditions, and determination of their metal content. The geochemical characteristics of Dağbaşı granitoid were also investigated because of the relationship between the geochemical features of the granitoids and skarn types and the metal contents. In addition, the compositions of sulfur minerals (pyrrhotite, pyrite, chalcopyrite, sphalerite, and galena) in skarn zones were measured by mineral chemistry analysis and the main and trace element contents were evaluated.

## 2. General Geology

The oldest units in the study area are volcano-sedimentary rocks consisting of andesite, basalt, and their pyroclastics including sandstone, marl, claystone, and sandy limestone intercalations. This unit is highly fractured and altered and covers a wide area around the Ipekçili, Köprüüstü, Kükürtlü, Çakırinsirt, and Kalaycıoğlu districts and Güney Hill. Andesites and basalts consist of plagioclase, amphibole, biotite, augite, and opaque minerals and display brecciated,

glassy, microlitic, microlitic porphyritic, amygdaloidal, and void textures. According to the microscopic study, the anorthite content of the plagioclases is  $An_{21-29}$  in andesite and  $An_{52-58}$  in basalt. In some cases, quartz, calcite, epidote, and chlorite, which are secondary in origin, accompany these minerals. In general, these secondary minerals are found along the fractures or gas cavities and are mostly accompanied by opaque minerals.

Pyroclastic rocks composed of tuff and volcanic breccia are observed as sedimentary intercalations in the volcanic rocks and are observed around the Çimenli, Akrut, and Ustaoglu districts. Tuffs are mainly composed of very small crystals and cementing ash, and breccias are made of relatively larger crystals, rocks fragments, and cementing ash material. Tuffs are classified as crystal and lithic crystal tuffs according to various mineral and rock fragments. In this unit, there are thin to medium laminated sandstone, marl, sandy limestone, and red biomicrite layers. They are a few metres in thickness and not more than several hundred metres in length.

This unit containing andesite, basalt, pyroclastics, and some sedimentary intercalations has been dated as Jurassic by Schultze-Westrum (1961), Köprübaşı (1992), and Çamur et al. (1994). Based on the *Involitina liassica*, *Trocholina* sp., *Lenticulina* sp., *Spirillina* sp., *Vidalina martana Farinacci*, *Lingulina* sp., and *Lagenidea* sp. fossil species found in the red biomicrite layer of the same unit, Liassic age was determined by Güven et al. (1998). On the other hand, Aydınçakır (2006) argues that volcano-sedimentary rocks may be Jurassic–Lower Cretaceous in age, taking into account the overlying Malm–Lower Cretaceous Berdiga formation.

Oldest volcanic rock units covering large areas around the Dağbaşı Granitoid (Figure 2) and extending along the eastern Black Sea metallogenic belt have been defined as Lower Basic Series by some researchers (Schultze-Westrum, 1961; Gedikoğlu et al., 1979; Aslaner, 1977; Şen, 1988; Kaygusuz, 1992; Aydınçakır, 2006). On the other hand, different names have been given to this volcano sedimentary unit, such as Telmeyaylası formation by Yüksel (1976), Hamurkesen formation by Açar (1977), Balkaynak formation by Kesgin (1983), Zimonköy formation by Eren (1983), and Şenköy formation by Kandemir (2004), although all these names refer to the Liassic same unit in the region according to

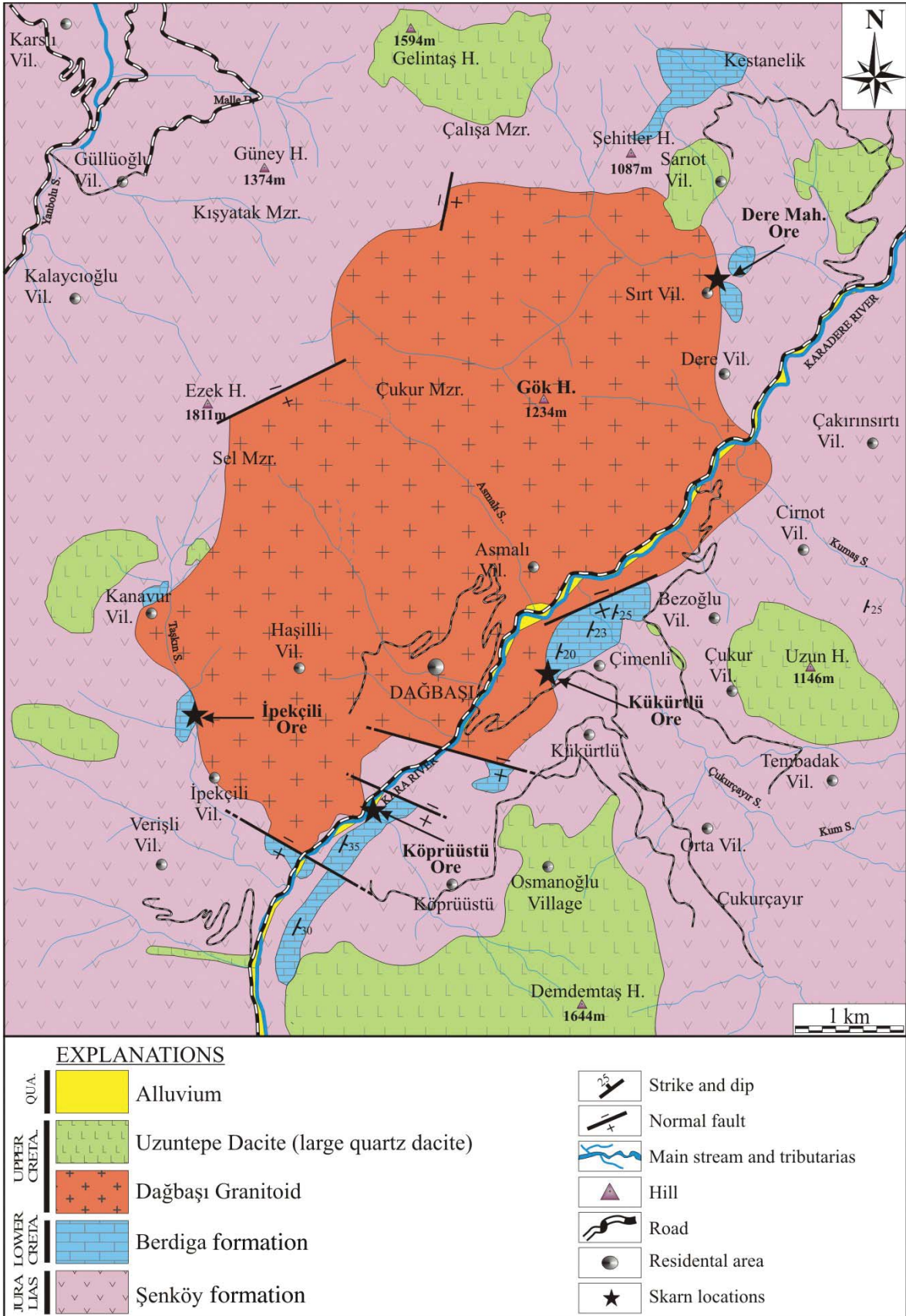


Figure 2- Geological map of the Dağbaşı area (Modified after Aydınçakır, 2006).

the palaeontological data. In this study, the name “Şenköy formation”, proposed by Kandemir (2004), is preferred, observing all the facies of this unit from bottom to top.

There are numerous dolomitic limestone lenses and blocks at the upper level of Şenköy formation, reaching up to 300 m in thickness and a kilometre in length. The thicknesses of the limestone layers cropping out around Sırt, Çiftepınar, Kestanelik, Kükürtlü, and Köprüüstü districts and Sel field vary between 10 and 30 cm. The colours of the limestones vary from dark grey to light grey far from the border, but the colours change in light colour tones from grey to beige near the granitoid contact, and calcite crystals become larger along the contact. These massive limestones, present in the northern part of the eastern Black Sea Region with limited lateral extensions, were considered as the products of platform carbonates and named as the Berdiga formation by numerous researchers (Kırmacı et al., 1996, 2018; Yılmaz et al., 2008). Limited lateral extension of these limestones was explained by active rifting tectonics during the Cretaceous by some studies (Yılmaz and Kandemir, 2006; Koch et al., 2008).

Carbonate and volcanic rock fragments, shell pieces, fine-grained quartz, plagioclase, and disseminated opaque minerals were observed in the thin section of the limestones. Significant lamination was observed at the levels containing clay-siltstone. Micritic cemented limestones were named as a biomicrite according to Folk (1962) and greywacke according to Dunham (1962). Although some *Globotruncana* and *Radiolarian* remnants were observed in some thin sections (the definition was given by Dr. Raif Kandemir), reliable palaeontological data could not be obtained in this study for the age determination. But it is understood that this unit was aged as Jurassic–Lower Cretaceous in some studies (Köprübaşı, 1992; Güven et al., 1998; Çamur et al., 1994), and this age was also accepted by some other researchers (Şen, 1988; Kaygusuz, 1992; Hasançebi, 1993; Aydınçakır, 2006; Kırmacı et al., 2018).

An outcrop of granitic rocks with an area of about 25 km<sup>2</sup>, around Dağbaşı region, was named as Dağbaşı Granitoid by Şen (1988). This granitoid was emplaced into volcano-sedimentary rocks of the Şenköy formation and crystallized limestones of the Berdiga formation (Figure 2). Quartz, plagioclase, alkali feldspar, pyroxene and amphibole minerals could

be observed in the granitic rocks macroscopically. Orthoclase ratios increase quite noticeably in the central part of the granitoid. Therefore, dark pink and pink-like grey colours become noticeable. The large crystal size in this central part becomes smaller towards the edge of the granitoid. Accordingly, the orthoclase contents decrease in the outer part of the granitoid while the quartz and plagioclase contents increase. Dağbaşı Granitoid contains some mafic microgranular enclaves, a few centimeters to a meter scale, along the contact with volcanic rocks. The age of the pluton was determined as 88.1–86.0 million years by Kaygusuz and Aydınçakır (2011) by the U–Pb SHRIMP method conducted on the zircon minerals. This time interval corresponds to the Upper Cretaceous period.

Dağbaşı Granitoid was divided into four different zones according to its modal mineralogical composition by Aydınçakır (2006). According to this study, monzogranite composition is dominant in central parts, while granitoid becomes granodiorite, tonalite, and diorite composition towards the outer zone. Because of the irregular distribution of these zones, additional sampling has been carried out to determine the petrographic and geochemical properties of the granitoids around the skarn contacts. In addition to macroscopically determined quartz, plagioclase, and alkali feldspar, hornblende and biotite were extensively observed in the prepared thin sections. Apatite and zircon are relatively less common and have euhedral crystal forms. Epidote and chlorite, observed especially around the biotites, are secondary in origin. Porphyritic and myrmekitic textures are quite common in thin sections. In some cases, biotite and hornblende inclusions in orthoclase minerals display poikilitic textures.

The dacitic rocks cutting Dağbaşı Granitoid and volcanic rocks of Şenköy formation around the study area were described as “coarse crystal dacites” by some studies (Şen, 1988; Kaygusuz, 1992; Hasançebi, 1993). On the other hand, as these dacites have characteristic columnar structure around Uzuntepe area, they were called “Uzuntepe Dacites” and Senonian age was appointed by Aydınçakır (2006) and Kaygusuz and Aydınçakır (2011).

### 3. Analytical Method

In this study, skarn zones around the Dağbaşı area have been systematically sampled. Preparations of thin and polished sections, mineralogical studies, and

sample preparation for the whole rock analyses have been carried out in the laboratories of the Department of Geological Engineering at the Recep Tayyip Erdoğan University.

Chemical analyses of 20 samples from the Dağbaşı Granitoid have been analysed for major, trace, and lanthanum group elements in the ACME analytic laboratory in Canada. Major and trace elements of the samples were analysed by ICP-AES (Inductively Coupled Plasma – Atomic Emission Spectrometry), and lanthanum group elements were analysed by the ICP-MS (Inductively Coupled Plasma – Mass Spectrometry) method. For the major and trace element analyses, 0.2 g of powdered sample was mixed with 1.5 g of  $\text{LiB}_2$ , then dissolved in 5%  $\text{HNO}_3$ -containing liquid, and then analysed. For lanthanum group element analyses, 0.25 g powdered samples were dissolved in various acidic solutions and then analysed. The results of the major element analyses are given as weight percentages, while trace and lanthanum group elements are given parts per million (ppm).

Silicate and sulfur mineral analyses have been carried out using a CAMECA-SX100 electron microprobe at the Mineralogy and Petrology Institute of Ludwig Maximilian University. Measurements were performed under conditions of 15 kV and 20 nA, and the electron beam diameter was chosen to be 1  $\mu\text{m}$ . The counting time was 30 s for Al, Ni, and Ca, 20 s for Ti, and 10 s for all the other elements. Natural and synthetic standards have been used for the calibration. The detection limit of the measured elements (in wt%) of the oxide samples was determined as 0.01 for Si, Al, K, Ti, Ca, and Na; 0.02 for Mg; 0.03 for Cr; 0.04 for Fe and Ni; and 0.06 for Mn. The detection limit for the sulfide samples was determined as 0.08 for the Fe, Pb, and S; 0.06 for the Cu; 0.05 for the As, Co, and Ni; 0.04 for Zn; 0.03 for Cd; and 0.02 for Ag.

#### 4. Studies in Skarn Zones

##### 4.1. Skarn Zones and Skarn Mineralogy

Four different skarn-type mineralizations were described around the Dağbaşı area including İpekçili, Köprüüstü, Kükürtlü, and Dere districts (Figure 3). There are some abandoned adits left from the old mining activities, all of which are closed. All the

skarn mineralizations have developed in the sides of the lens- and block-shaped limestones closest to the pluton. The contact between granitoid and limestones is not observable in the area (Figure 3). There are no skarn developments in the granite itself, so all of the skarns have developed as exoskarn. Considering the mineralogy and texture of the skarn, four zones have been studied accordingly. As İpekçili and Köprüüstü skarns have similar characteristics, they have been considered together. In these locations, a progressive stage is represented by the presence of garnets and pyroxenes. According to their textures, they have been divided into early and late stages and the minerals of both stages have been defined in the distal zone limestones. Early progressive stage garnets and pyroxenes together show massive (Figure 4a), rhythmically banded (Figure 4b), nodular (Figure 4c), and granular (Figure 4d) textures representing primary developments. These first stage garnets show zoned growth structures under the microscope (Figure 4e) and in the BSE pictures (Figure 4f). Late progressive stage garnets and pyroxenes have developed as veins along the cracks in the limestones (Figure 4g) and they also show zoned growth under the microscope (Figure 4h) and in the BSE pictures (Figure 4i). Early stage garnets do not have any relation with the ore-forming minerals; on the other hand, late stage garnets accompany to magnetite and hematite in their growth zones (Figure 4j), indicating that ore mineralizations started in the late stage. Quartz and calcite always accompany to the prograde stage garnets and pyroxene in thin sections.

In these two locations, retrograde stage skarn minerals of epidote, quartz and calcites have developed along the fractures of volcanic host rocks (Figure 4k, l). In some locations, retrograde stage epidote and quartz are also present as disseminations in the volcanic rocks (Figure 5a). In the Köprüüstü location only, retrograde stage minerals, that is, tremolites and actinolites, have garnet and pyroxene as macro-lenses (Figure 5b) and as micro-inclusions (Figure 5c).

In the Kükürtlü and Dere Mahalle districts, garnet and pyroxene developments, representing prograde stage, are not seen in thin sections or macroscopically in the field. The signs of retrograde skarn developments are present in these locations. Developments of epidote, chlorite, quartz, and calcite veins are commonly present (Figure 5d) in these two locations along the cracks in the limestones and volcanic rocks. In some cases, banded structures are present (Figure 5e) between quartz and epidote. In addition, there are

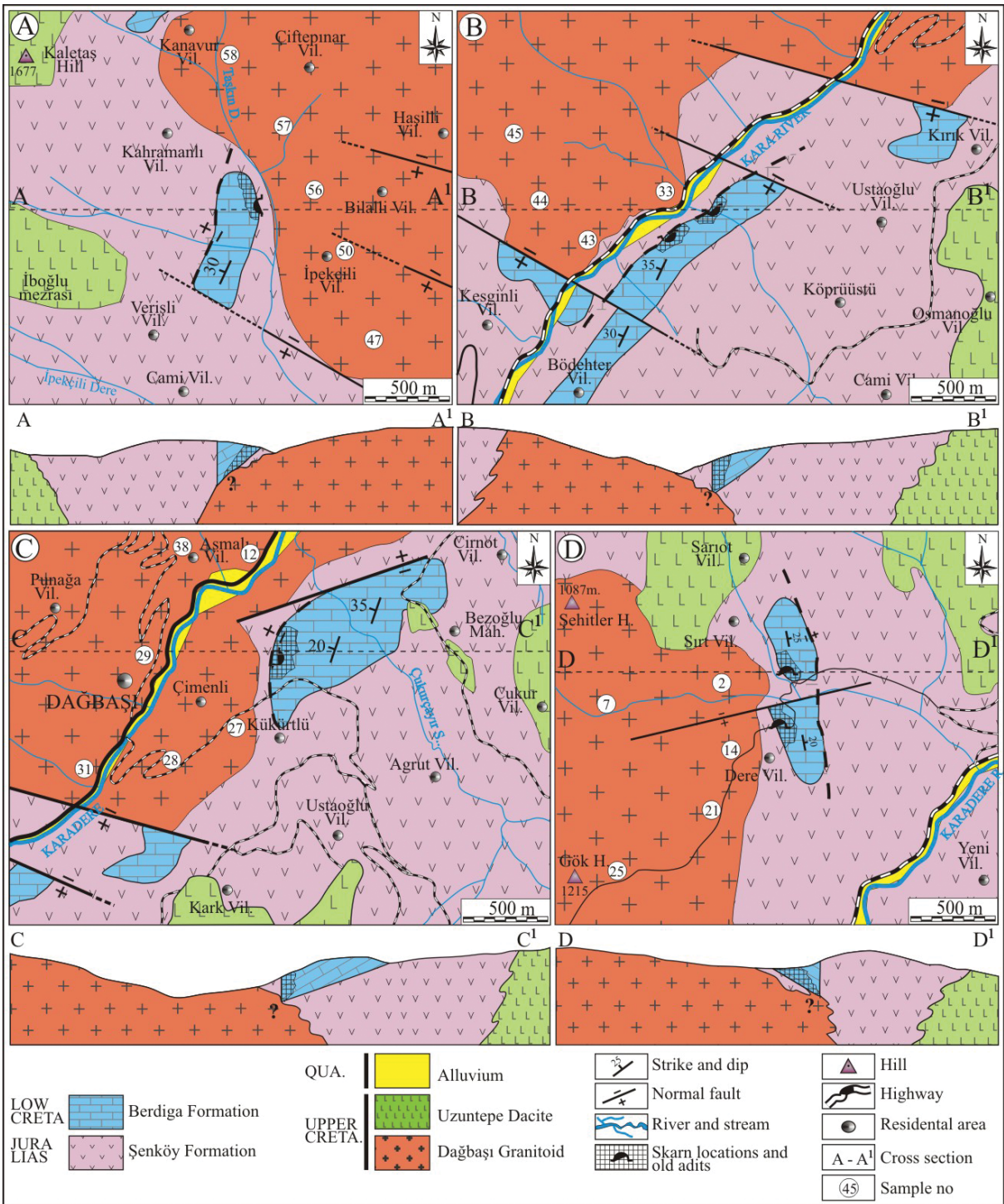


Figure 3- a) Geological map and cross sections of the skarns in İpekçili, b) Köprüüstü, c) Kükürtlü, d) Dere Mahalle locations (Modified after Aydınçakır, 2006).

quartz inclusions, reaching up to 1 cm in size, in both limestones and volcanic rocks (Figure 5f). In the thin sections, early epidotes always accompany the quartz (Figure 5g), and the quartz was enclosed by later stage epidotes. In the thin sections, quartz and calcite are

commonly observed in the fractures (Figure 5h) and gas voids (Figure 5i) of volcanic host rock.

Oxide and sulfur minerals in the outcrops in the İpekçili and Köprüüstü locations have different

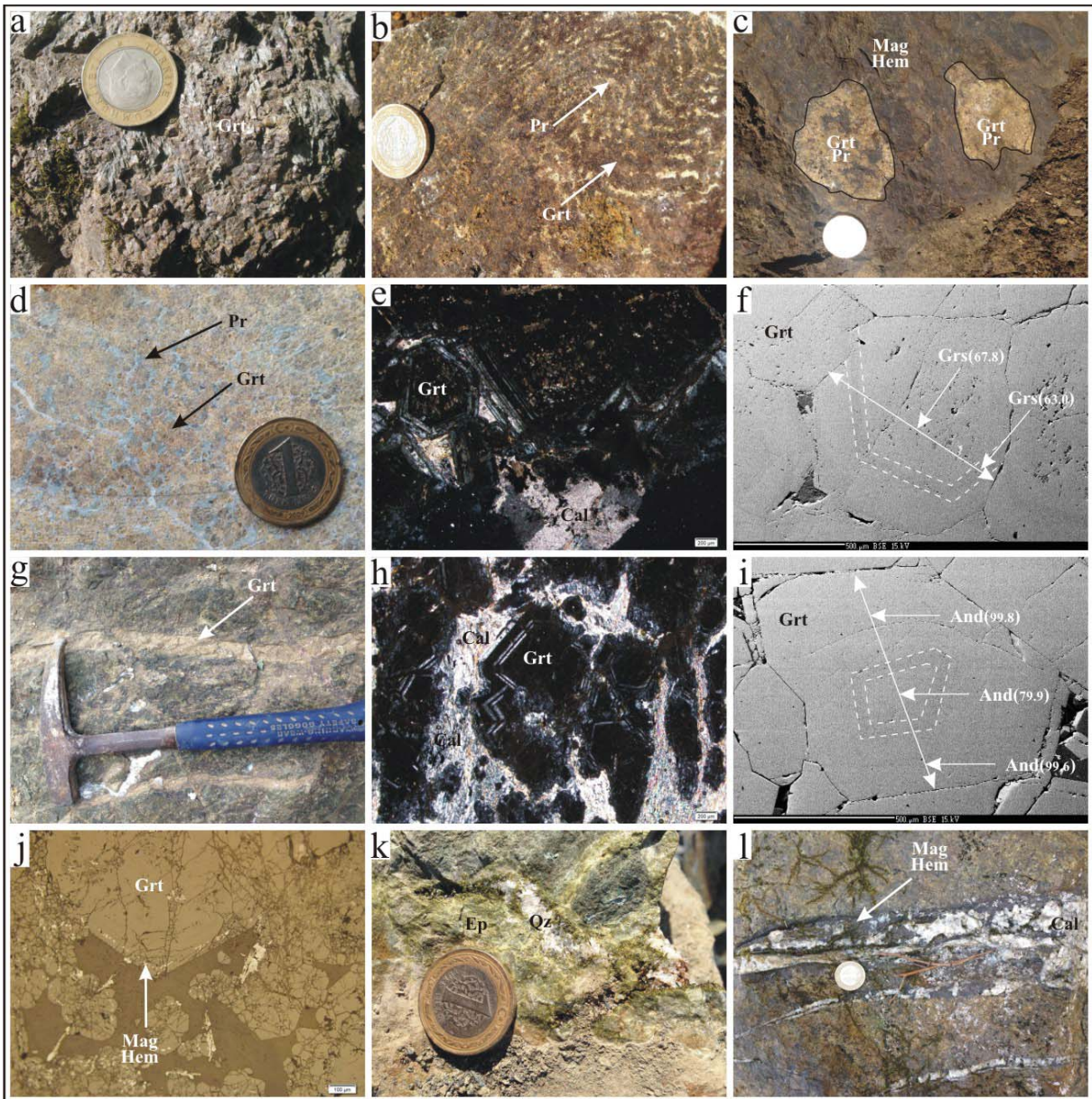


Figure 4- a) Massive garnet texture in the İpekçili skarn; b) rhythmically banded texture between garnet and pyroxenes; c) nodular garnet and pyroxenes in the Köprüüstü carbonates; d) granular texture showing that garnet and pyroxenes developed together; e, f) microphotograph and BSE photograph of early stage zoned garnet crystal (X nicol); g) late stage garnet veins developed along the cracks in the limestones (rarely including pyroxene); h, i) microphotograph (X nicol) and BSE photograph of zoned late stage garnet (X nicol); j) magnetite and hematite developments along the growth zone of late stage garnets; k) epidote and quartz developments in the volcanic rocks during the retrograde skarn stage; l) magnetite- and hematite-bearing calcite veins in the volcanic host rocks (Grt: garnet; Pr: pyroxene; Mag: magnetite; Hem: hematite; Qz: quartz; Cal: calcite; Trm: tremolite; Act: actinolite; Ep: epidote).

structures. These are irregularly shaped piles (Figure 6a) and lenses in the limestones, banded along the weak zones of limestone layers with a thickness of up to 30 cm in size (Figure 6b), irregularly shaped fracture-filling type in the limestones with a thickness not exceeding 10 cm (Figure 6c), and fracture-filling and breccia-filling structures in the volcanic host rock (Figure 6d). Along these zones, epidote, quartz, and

calcite accompany ore minerals. However, magnetite and hematite developments in growth zones in the late stage garnets indicate that ore mineralization started towards the end of the prograde stage (Figure 4j). On the other hand, both the ore shape and the presence of epidote, quartz, and calcite accompanying ore mineralization indicate that the main ore mineralization developed at the retrograde skarn stage.

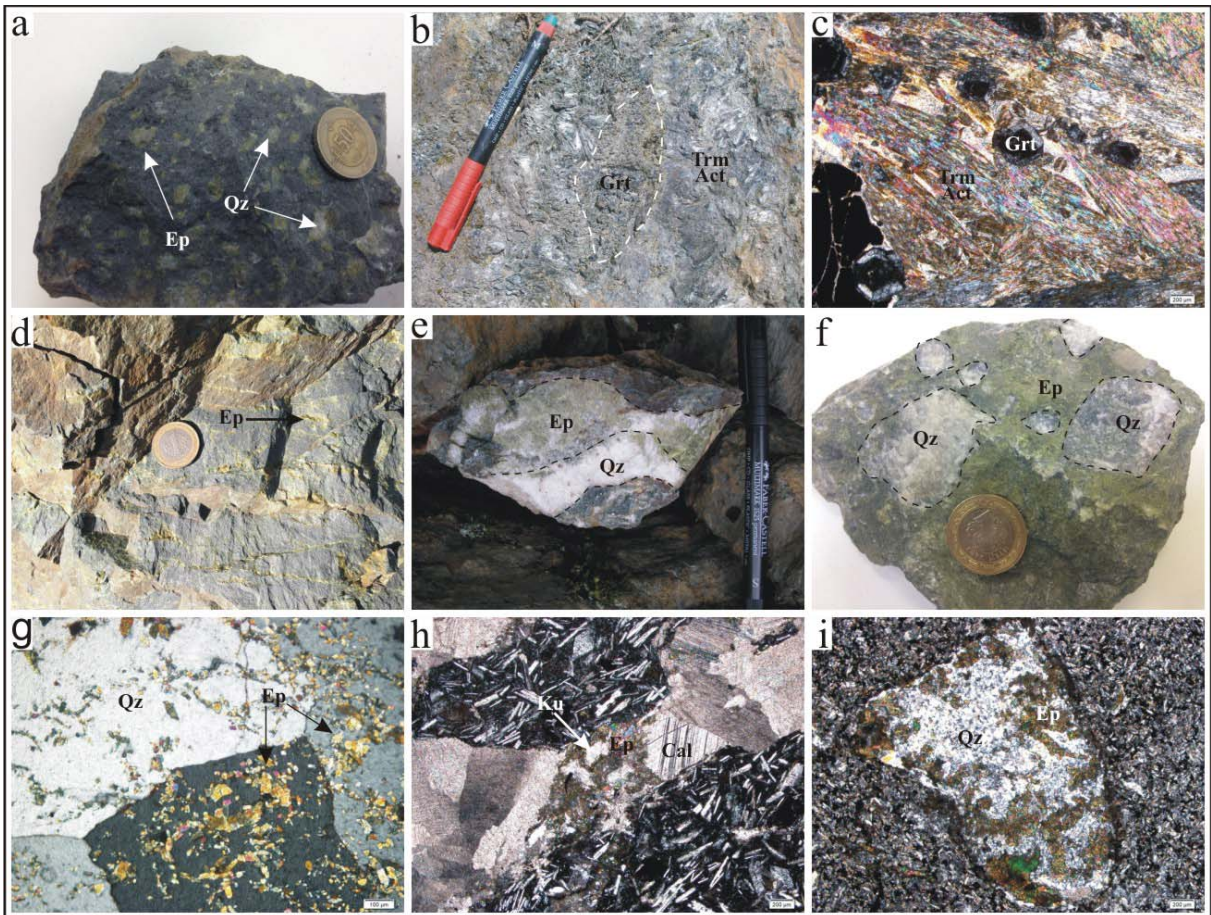


Figure 5- a) Epidote and quartz disseminations in the volcanic host rocks; b) garnet and pyroxene inclusions in the tremolites and actinolites of the Köprüüstü skarn; c) microphotograph of (X nicol) garnet inclusions in the tremolites and actinolites; d) epidote, quartz, and calcite veins developed along the cracks of the volcanic host rock around the Kükürtlü and Dere mahalle districts; e) banded texture of quartz and epidote; f) quartz inclusions in the highly epidotized volcanic rocks; g) microphotograph (X nicol) of quartz and epidote development; h and i) microphotograph (X nicol) of epidote, quartz, and calcite developments along the cracks and gas voids in the volcanic rocks (Qz: quartz; other symbols are same as it is in figure 4).

In the Kükürtlü and Dere Mahalle locations, in addition to magnetite and hematite veins formed along the fractures of limestone and volcanic host rock, ellipsoidal magnetite and hematite piles, up to meter in size, were also observed (Figure 6e). Apart from these, disseminated magnetites and hematites can be seen in thin sections as well as in the hand specimens (Figures 6f, g). Replacement remnants of magnetite and hematite accompany quartz fillings seen in Figure 5f (Figure 6h). Ore mineralization in the Kükürtlü and Dere Mahalle locations developed at the retrograde stage, because evidence for a prograde skarn stage has not been identified. However, quartz and epidote are found to be filling fractured ore fragments, indicating that ore mineralization started before these minerals (Figure 6i).

Magnetites and hematites (in some cases as specularite) are the main ore-forming minerals in each location. Magnetites and hematites seen in the growth zones (Figure 4i) of the late stage garnets indicate that ore mineralizations started together with these late stage garnets. However, the presence of these garnets as inclusions in magnetites and hematites indicates that the main ore development takes place after these garnets (Figure 6j). Apart from magnetite and hematite, there is some difference in terms of the sulfur mineral content between locations. Pyrrhotite, pyrite, and chalcopyrite are the sulfur minerals present in the skarn zone in the İpekçili location. In this location, pyrrhotites are characteristic with a “bird’s eye structure” (Figure 6k) and have been replaced by late stage sphalerites (Figure 6l). In the Köprüüstü location, galena accompanies pyrite,

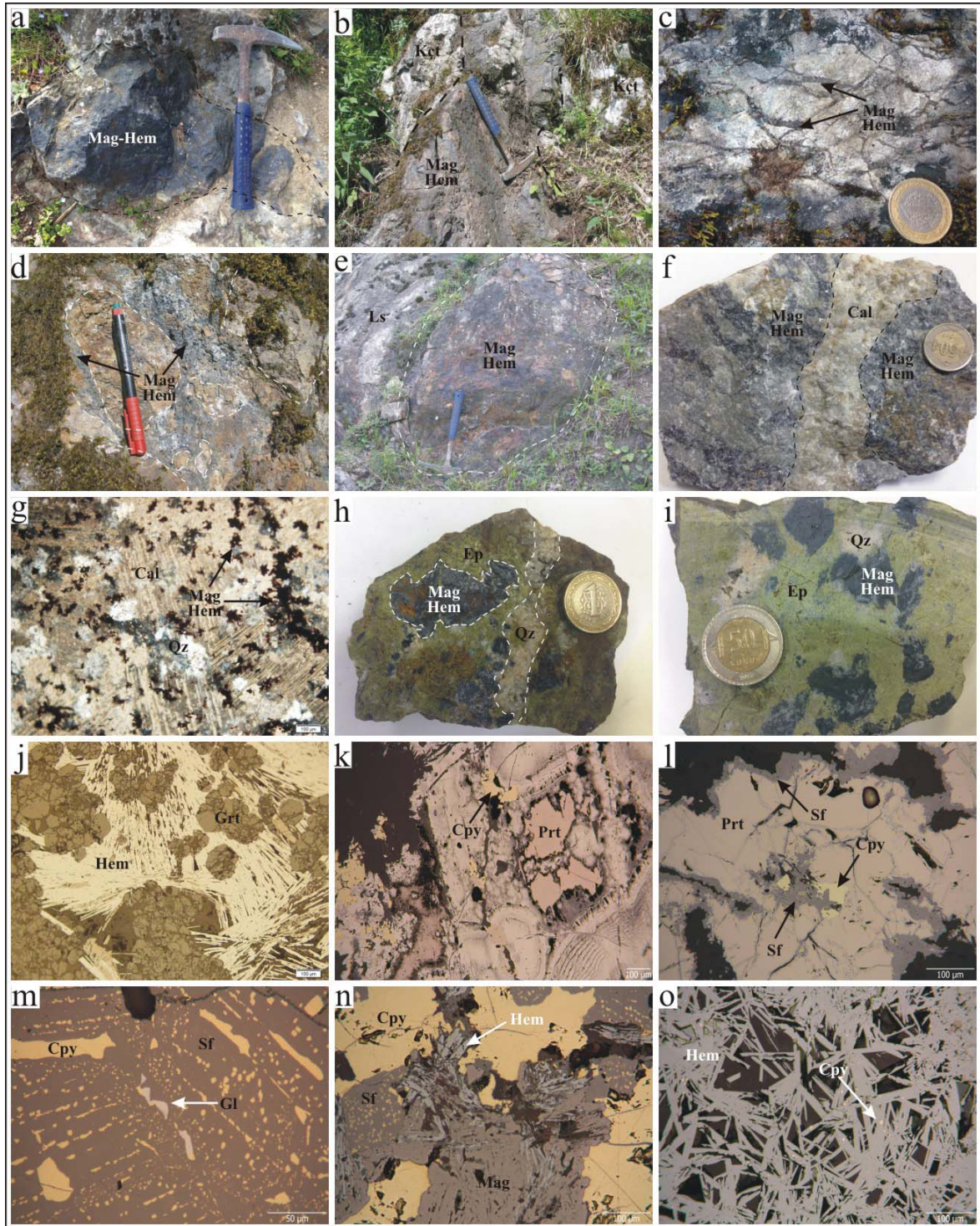


Figure 6- a) Ore pile containing unsystematically developed magnetite and hematite; b) magnetite and hematite development in the weak zones along the bedding planes in the limestones; c) ore veins developed along the fracture zones in the limestones; d) volcanic breccia filling structure along the skarn zones; e) ellipsoidal ore piles in the limestones reaches up to meter size; f, g) macro and micro (X nicol) photograph of magnetite and hematite disseminations along the calcite veins in the limestones; h) partly replaced ore inclusions in the epidotes; i) epidote and quartz filling the interspaces in the ore fragments; j) late stage garnet inclusions in the hematites; k) pyrrhotites with characteristic bird's eye texture, commonly found in the İpekçili skarn; l) replacements of pyrrhotites by sphalerites; m) exsolution texture between chalcopyrite and sphalerite is commonly present in the Köprüüstü skarn. Galena inclusion in the sphalerite; n) coexistence of oxide and sulfur minerals in the Köprüüstü skarn; o) pyrite and chalcopyrite inclusions in the hematites of the Kükürtlü skarn (Cpy: chalcopyrite; prt: pyrrhotite; sf: sphalerite; gl: galena; other symbols are same as it is in figure 4).

chalcopyrite, and sphalerite (Figure 6m) which is much less common than the others. Magnetites and hematites also accompany sulfide ore mineral (Figure 6n). However, these magnetites and hematites are in the form of mineral inclusions in the sulfur minerals. Alteration products of covellite, chalcocite, digenite, and goethite are present in both locations.

Magnetite and hematites are the main ore minerals in both Kükürtlü and Dere Mahalle locations. Pyrite and chalcopyrite inclusions, a few microns in size, are observed rarely in these minerals (Figure 6o). Apart from these, no other sulfide minerals are present. Abundances of the sulfide minerals in Kükürtlü and Dere Mahalle locations are much lower compared with the İpekçili and Köprüüstü ores. With all the information given on the skarn mineralogy, paragenesis and successions of the Dağbaşı skarn ore have been established as shown in figure 7.

4.2. Geochemical Characters of the Dağbaşı Granitoid and Their Relations with the Skarn Types

Dağbaşı Granitoid has different mineralogical and geochemical zonings (Aydınçakır, 2006). Because of irregular distribution of these zones, additional sampling and geochemical analyses were performed. For this purpose, 20 samples were collected from the skarn zone granitoids and were analysed for their major, trace, and LGE elements (Table 1) and results have been correlated with the skarn types. Chemical compositions of the granitoids along the skarn zones have been correlated with the chemical compositions of the granitoids in other parts and the results were

evaluated from the viewpoints of skarn types. SiO<sub>2</sub>, CaO, and Na<sub>2</sub>O values of the granitoid samples are in the following order: 61.76–71.69%, 2.32–4.88%, and 2.77–4.30%. Al<sub>2</sub>O<sub>3</sub> changes from 13.12 to 16.72% and K<sub>2</sub>O changes (apart from samples 12 and 38, which show variations from 0.45 to 0.82%) from 2.28 to 3.75%. Based on these values, A/NK and A/CNK ratios of 1.51–2.45 and 0.88–1.23, respectively, have been calculated.

Considering the major element content, granitoid samples show compositions between granodiorite and tonalite compositions (Figure 8a) in the P–Q diagram (Debon and Le Fort, 1988). However, granodiorite, monzogranite and tonalite samples collected from various and parts of the granitoid by Aydınçakır (2006) have tonalite compositions. Analyses of the samples collected by Aydınçakır (2006) and samples in this study fall into the calc-alkaline area in the AFM classification diagram (Figure 8b) of Irvine and Baragar (1971). While skarn-zone granitoids fall into the high-potassium calc-alkaline area in the SiO<sub>2</sub>–K<sub>2</sub>O diagram (Figure 8d), analyses of the samples collected from other parts of the granitoid fall into medium calc-alkaline and tholeiitic areas. According to the molar A/NK and A/CNK ratios, samples from the skarn zones have metaluminous–peraluminous compositions, while samples from the other parts have peraluminous compositions (Figure 8e). Comparing the major element analyses of the skarn-zone granitoids with the skarn-producing granitoids of different types (Figures 8c, d), all the samples have compositions between the Fe–Cu–Zn type skarn (Meinert et al., 2005). On the

Minerals	Prograde Stage		Retrograde Stage	Supergene
	Early	Late		
Garnet	_____	_____		
Pyroxene	_____	_____		
Trem-Actin.			_____	
Epidote			_____	
Calcite				_____
Quartz		_____		_____
Magnetite			_____	
Hematite			_____	_____
Pyrrhotite			_____	
Pyrite			_____	
Chalcopyrite			_____	
Sphalerite			_____	
Galena			_____	
Covellite				_____
Chalcocite				_____
Digenite				_____
Goethite				_____

Figure 7- Generalized mineral paragenesis and succession in the skarn ores around Dağbaşı area.

Table 1- Major oxide (wt%), trace and LGE elements (ppm) content of the samples from the skarn zone granitoid.

Sample No	2	7	12	14	21	25	27	28	29	31	33	38	43	44	45	47	50	56	57	58
Major oxid (%)																				
SiO <sub>2</sub>	62.94	63.69	71.69	62.86	63.18	65.10	64.25	63.26	65.66	65.19	64.62	71.21	63.15	61.76	63.30	63.70	64.53	65.48	63.04	62.73
TiO <sub>2</sub>	0.39	0.38	0.30	0.39	0.38	0.34	0.37	0.39	0.33	0.32	0.37	0.33	0.40	0.40	0.37	0.38	0.39	0.36	0.40	0.38
Al <sub>2</sub> O <sub>3</sub>	16.10	15.70	14.54	16.18	15.65	14.99	15.66	15.45	15.32	15.21	16.72	13.12	15.40	15.37	16.01	15.59	16.37	14.91	14.66	15.92
Fe <sub>2</sub> O <sub>3</sub>	4.62	4.42	2.07	4.73	4.48	3.92	4.26	4.50	4.14	3.93	4.32	3.79	4.62	4.66	4.43	4.54	4.42	4.15	4.69	4.50
MnO	0.13	0.11	0.02	0.13	0.11	0.10	0.11	0.11	0.11	0.10	0.11	0.08	0.12	0.12	0.11	0.11	0.13	0.11	0.12	0.11
MgO	1.92	1.96	1.17	2.04	2.00	1.64	1.83	1.97	1.61	1.65	1.70	0.86	2.51	2.73	2.14	2.35	1.72	1.79	2.14	2.01
CaO	4.88	4.25	4.30	3.71	4.12	4.13	4.31	4.47	3.81	3.89	2.32	3.00	2.70	3.95	3.46	3.74	4.61	2.70	3.89	3.22
Na <sub>2</sub> O	3.38	3.07	3.68	3.65	3.83	3.16	3.13	3.38	3.54	3.70	3.47	4.30	4.03	3.26	3.40	3.44	3.64	2.77	3.09	4.26
K <sub>2</sub> O	2.41	3.03	0.45	3.07	2.78	2.68	2.55	2.71	2.38	2.89	2.43	0.82	3.19	3.24	3.38	3.20	2.47	3.75	2.28	3.45
P <sub>2</sub> O <sub>5</sub>	0.13	0.13	0.07	0.14	0.13	0.11	0.12	0.13	0.11	0.12	0.13	0.07	0.13	0.14	0.13	0.14	0.13	0.13	0.13	0.13
LOI	2.80	3.00	1.50	2.80	3.00	3.50	3.10	3.30	2.70	2.70	3.60	2.30	3.40	4.00	2.30	2.50	1.30	3.60	5.30	3.00
Total	99.70	99.68	99.78	99.68	99.69	99.68	99.66	99.67	99.71	99.71	99.75	99.83	99.69	99.61	99.68	99.67	99.69	99.70	99.72	99.73
A/NK	2.17	2.45	1.72	1.74	1.68	1.94	1.96	1.85	1.77	1.71	1.79	1.53	1.58	1.81	1.59	1.75	1.70	1.97	1.86	1.51
A/CNK	0.88	1.06	0.90	0.97	0.91	0.99	0.98	0.93	0.98	0.96	1.21	1.00	1.06	0.99	0.98	1.01	0.90	1.23	1.03	0.99
Tra. Ele. (ppm)																				
Ni	1.80	1.70	0.60	1.10	1.50	1.70	1.70	1.60	1.00	1.00	1.60	<0.1	8.10	8.90	6.60	7.40	1.40	1.40	2.10	2.30
V	94.00	99.00	50.00	104.00	102.00	85.00	93.00	100.00	84.00	89.00	87.00	27.00	96.00	107.00	99.00	107.00	85.00	93.00	99.00	103.00
Cu	8.40	9.00	1.10	9.40	12.50	12.80	12.60	13.60	9.80	9.20	10.00	1.00	8.20	2.50	12.90	14.30	8.00	16.30	24.30	14.70
Pb	2.50	2.60	0.50	5.20	3.30	13.10	10.40	2.80	7.70	2.50	10.20	1.30	4.00	4.50	7.50	6.40	5.70	49.50	72.80	5.30
Zn	46.00	43.00	6.00	33.00	46.00	37.00	43.00	42.00	37.00	37.00	46.00	40.00	47.00	50.00	36.00	38.00	27.00	46.00	118.00	47.00
W	254.00	375.80	749.90	283.70	234.60	275.70	224.10	296.10	163.20	129.40	207.60	555.50	157.50	299.60	172.60	272.10	359.00	159.50	156.00	230.10
Rb	57.10	74.70	6.10	81.30	67.30	73.40	64.20	59.50	62.30	64.30	75.10	14.70	84.90	85.70	85.50	79.40	61.60	123.80	69.10	84.90
Ba	1136.00	1129.00	143.00	1206.00	1205.00	1379.00	1494.00	1317.00	1297.00	1317.00	782.00	230.00	1275.00	1604.00	1331.00	1223.00	1115.00	1468.00	1043.00	1029.00
Sr	523.20	520.70	385.70	596.30	530.40	509.70	553.70	515.50	501.60	527.20	495.40	229.00	413.40	518.00	568.60	574.80	556.30	388.00	273.50	393.00
Ta	0.60	0.70	0.50	0.60	0.60	0.60	0.60	0.70	0.70	0.60	0.60	0.20	0.70	0.70	0.60	0.60	0.60	0.60	0.50	0.50
Nb	8.00	7.60	5.20	7.80	7.60	7.50	8.10	7.50	7.80	6.60	8.10	2.80	7.40	7.00	6.80	7.00	7.90	7.10	7.20	7.20
Hf	2.60	2.90	2.90	2.90	2.80	2.50	2.60	2.60	2.50	2.50	3.00	3.00	2.90	2.70	2.60	2.50	2.70	2.60	2.40	2.60
Zr	106.20	106.80	98.00	104.90	104.10	87.60	94.50	93.60	96.40	81.50	104.20	120.10	96.90	103.30	96.30	90.70	100.50	104.30	95.00	91.30
Y	12.50	11.30	17.20	15.60	12.10	10.80	12.10	11.80	11.00	9.40	13.40	27.90	15.20	12.60	12.00	12.10	13.00	12.40	11.10	11.60
Th	6.70	8.80	6.60	8.80	8.60	9.90	8.70	8.60	7.90	9.30	6.70	2.00	9.90	9.20	9.70	9.30	7.10	6.70	9.30	9.40
U	2.70	2.60	1.80	2.70	2.90	2.90	2.90	3.10	2.60	2.70	2.20	0.70	2.60	2.80	2.80	2.90	2.40	2.30	2.90	2.70
LGE (ppm)																				
La	26.40	28.00	19.50	29.00	26.80	27.80	27.20	27.90	28.50	25.00	28.00	10.10	33.10	24.20	28.50	28.60	31.30	22.90	23.60	22.90
Ce	46.40	45.50	34.50	47.50	45.80	46.20	45.60	45.10	47.60	42.50	46.90	21.10	51.10	42.60	47.30	48.70	55.60	43.50	42.30	42.50
Pr	4.73	4.68	3.60	5.12	4.50	4.47	4.58	4.73	4.71	4.07	5.18	2.60	5.38	4.48	4.60	4.78	5.51	4.32	4.40	4.18
Nd	16.70	16.20	13.50	19.10	15.60	15.70	15.90	16.10	16.10	13.80	18.50	12.00	20.30	16.10	15.40	16.70	18.60	14.70	16.30	14.70
Sm	2.90	2.83	2.41	3.19	2.66	2.63	2.64	2.71	2.67	2.38	3.18	2.94	3.02	2.67	2.77	2.79	2.93	2.51	2.62	2.50
Eu	0.80	0.74	0.71	0.86	0.77	0.70	0.80	0.80	0.80	0.70	0.91	1.05	0.94	0.82	0.81	0.83	0.85	0.65	0.63	0.71
Gd	2.71	2.46	2.71	3.19	2.57	2.20	2.34	2.61	2.18	2.10	2.68	3.91	3.08	2.59	2.62	2.56	2.71	2.37	2.14	2.17
Tb	0.35	0.31	0.40	0.43	0.35	0.32	0.33	0.35	0.33	0.29	0.40	0.65	0.40	0.36	0.32	0.35	0.37	0.34	0.32	0.31
Dy	2.22	1.94	2.66	2.52	2.06	1.94	2.02	1.89	1.80	1.70	2.22	4.31	2.22	2.16	1.87	2.16	2.11	1.95	1.99	1.90
Ho	0.42	0.39	0.56	0.51	0.41	0.39	0.38	0.43	0.40	0.34	0.45	1.02	0.45	0.39	0.38	0.39	0.44	0.39	0.40	0.34
Er	1.31	1.12	1.71	1.52	1.15	1.18	1.12	1.24	1.10	1.12	1.18	2.99	1.46	1.26	1.18	1.20	1.33	1.20	1.13	1.11
Tm	0.21	0.18	0.27	0.22	0.17	0.18	0.17	0.18	0.17	0.15	0.21	0.46	0.21	0.19	0.18	0.20	0.21	0.20	0.18	0.18
Yb	1.27	1.26	1.80	1.40	1.33	1.14	1.35	1.38	1.24	0.98	1.30	2.93	1.28	1.16	1.20	1.32	1.33	1.25	1.15	1.13
Lu	0.22	0.20	0.29	0.23	0.19	0.19	0.20	0.21	0.20	0.20	0.24	0.49	0.23	0.21	0.21	0.18	0.22	0.19	0.19	0.19

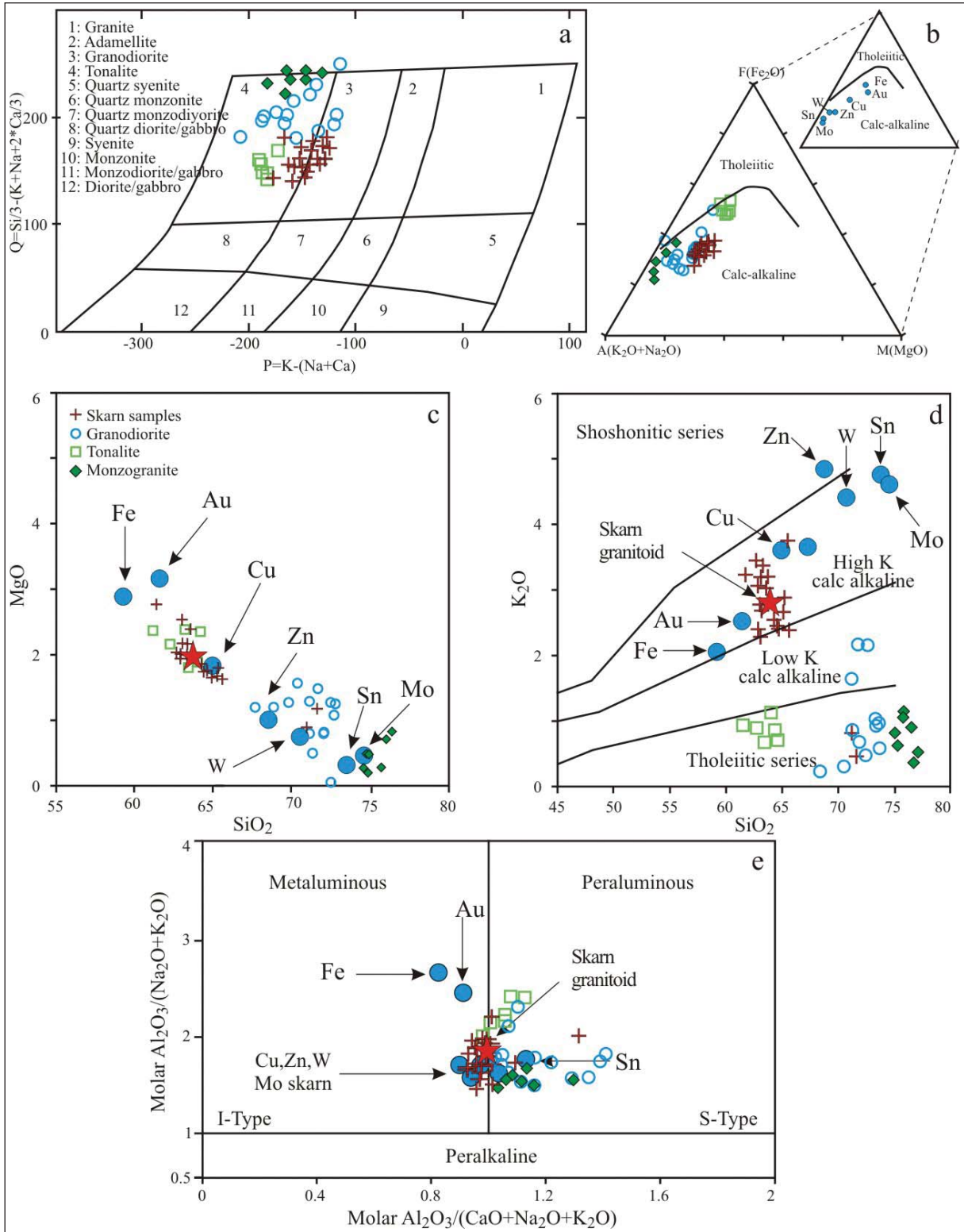


Figure 8- a) Distribution pattern of the skarn zone granitoid samples and samples from the other part of the Dağbaşı Granitoid plotted together on the P-Q diagram (Debon and Le Fort, 1983); b) distribution of these samples on the AFM diagram and comparison of these samples with the skarn-related granitoids (tholeiitic-calc-alkali curve according to Irvine and Baragar, 1971); c, d) MgO and  $\text{K}_2\text{O}$  variations of these samples versus  $\text{SiO}_2$  and comparison of these samples with the skarn-related granitoids; e) classification based on molar A/NK versus A/CNK transition (Maniar and Piccoli, 1989). The star symbol is the average of the skarn granitoid samples.

other hand, the results of the samples from the other parts of the Dağbaşı Granitoid collected by Aydınçakır (2006) show quite different composition from the skarn-producing granitoids.

Changes in major element contents of the skarn zone granitoids have been correlated with the  $\text{SiO}_2$  contents. There was no meaningful outcome. However, when the results of this study were evaluated together with the results of Aydınçakır (2006), the increase in  $\text{SiO}_2$  contents showed negative correlations with the  $\text{K}_2\text{O}$ ,  $\text{CaO}$ ,  $\text{MgO}$ ,  $\text{Al}_2\text{O}_3$ ,  $\text{Fe}_2\text{O}_3$ ,  $\text{P}_2\text{O}_5$ , and  $\text{TiO}_2$  contents (Figure 9a, c–h.) On the other hand, there is a positive correlation between the  $\text{SiO}_2$  and  $\text{Na}_2\text{O}$  contents (Figure 9b). The negative correlation between  $\text{SiO}_2$  and  $\text{MgO}$ ,  $\text{CaO}$ , and  $\text{Al}_2\text{O}_3$  represents the fractional crystallization of plagioclase, hornblende, and biotite; the correlation between  $\text{SiO}_2$  and  $\text{Fe}_2\text{O}_3$  and  $\text{TiO}_2$  represents the magnetite and Ti-oxide fractions; and the correlation between  $\text{SiO}_2$  and  $\text{P}_2\text{O}_5$  represents the apatite fractions. All of the negative correlations for the major elements indicate that the granitoid originated from the parent reservoir by fractional crystallization.

Granitoid samples from the skarn zones fall into the volcanic-arc-type granitoid (VAG) field in the tectonic setting classification diagrams of Nb–Y and Rb–Y+Nb (Figures 10a, b). Nb–Y, Rb–Y+Nb, and Rb–Sc diagrams show that the trace element content of the skarn granitoid has a similar composition to the Fe–Cu–Zn-type skarn-producing granitoids (Figures 10a, b, and d). On the other hand, the distribution of the samples from the other parts of the granitoid displays a quite independent composition pattern. Based on the analyses of the samples of the zoned Dağbaşı Granitoid, near to skarn zones, these graphics show that an association could be drawn between the skarn types and the compositions of the Dağbaşı Granitoid. On the other hand, samples from the other parts of the granitoid do not have any compositional similarities with the skarn types. Both granitoid samples close to the skarn zones and samples from other parts of the granitoid have similarities with the Fe–Cu–Zn-type skarn composition on the Rb/Sr–Zr diagram (Figure 10c).

#### 4.3. Compositions of the Skarn Minerals

Skarn-type deposits develop by metasomatic processes along the contacts between carbonate rocks and granitic intrusions. The mineralogical properties of

the skarn show differences according to the chemical composition of the magma, type of carbonate host rock, depth of the skarn development, and degree of oxidation of skarn minerals (Meinert et al., 2005). Because of this, the mineralogical properties of the skarns have to be taken into account when defining and classifying skarn-type deposits. Additionally, the chemical compositions of the minerals and their zonations give valuable information on the process and environment of skarn development.

Garnets and pyroxenes are the most common minerals present in the skarn zones. Studies on skarn deposits showed that there is a systematic connection between the compositions of these minerals and the metal contents of the deposits. So classifications have been carried out on the basis of the compositions of these minerals (Burt, 1972, 1982; Einaudi et al., 1981; Nakona et al., 1994, 1998; Meinert et al., 2005). The stoichiometric compositions of these minerals determined by analysing their compositions are commonly shown as end members on the triangular diagrams. In these studies (pyrope+spessartine+almandine)–grossular–andradite are used as end members for garnet, and johannsenite–hedenbergite–diopside are used as end members for pyroxenes.

In this study, the compositions of the garnet and pyroxenes in the skarn zones have been analysed by electron-probe micro analyser (EPMA) and their chemical stoichiometric compositions and end members have been calculated. Skarn types have been determined by plotting these data on triangular diagrams. Additionally, the chemical variations of petrographically determined early and late stage minerals and variations on the zoned crystals have been studied. Those, evolutions of the solutions caused skarns have been investigated. The calculations are based on a total of 24 oxygens for garnets and six oxygens for pyroxenes. The ferric iron calculation for garnets has been carried out according to Droop (1987).

##### 4.3.1. Garnet

Analyses of garnets from Köprüüstü and İpekçili locations have been evaluated and early and late stage garnet compositions have been interpreted separately. Analyses of the garnets from these two locations are given in table 2. Early garnets from the Köprüüstü location are dominantly of grossular type and have the

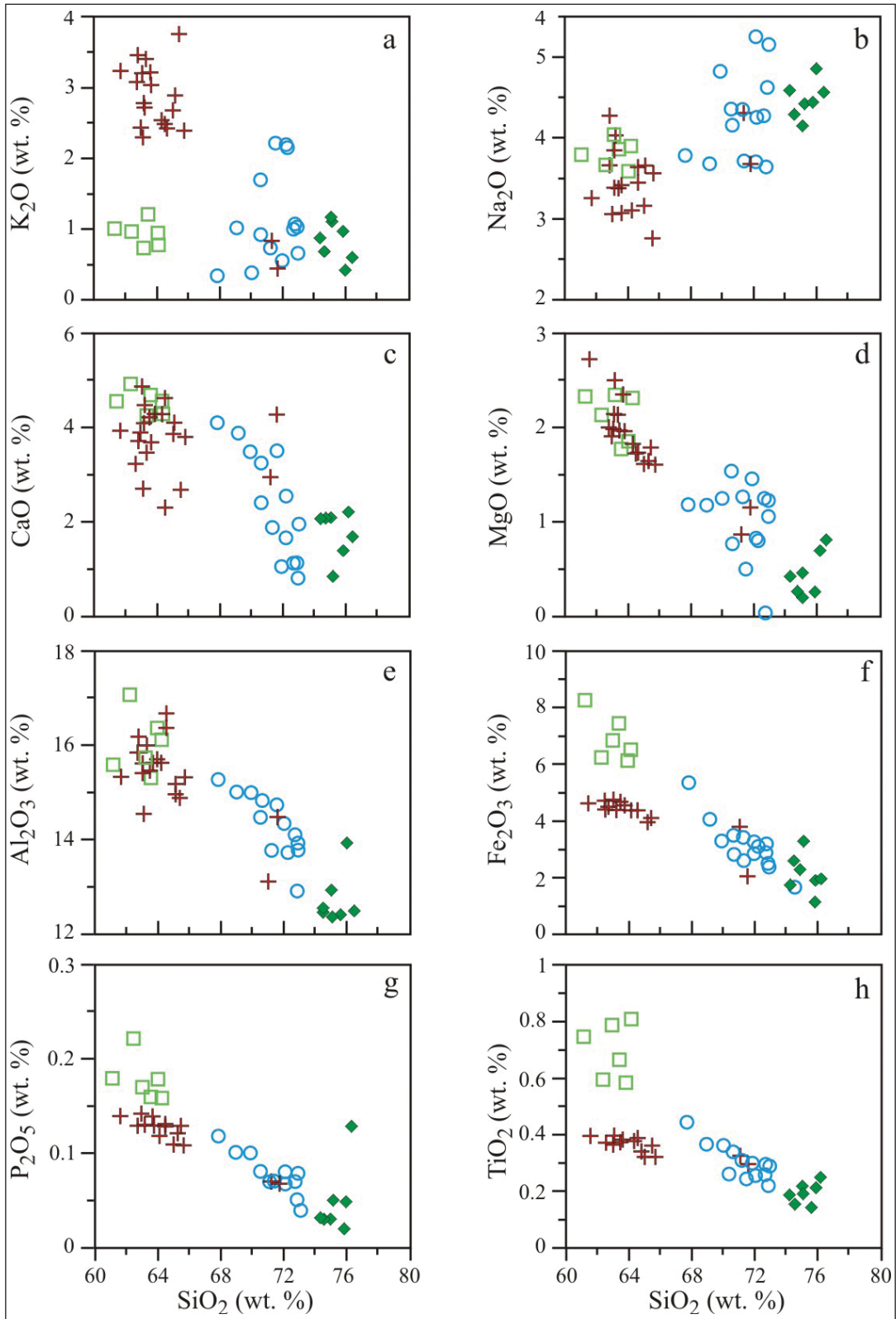


Figure 9- SiO<sub>2</sub> versus major element variation diagrams of the samples from the skarn zones and other parts of the granitoid (symbols are same as it is in figure 8c).

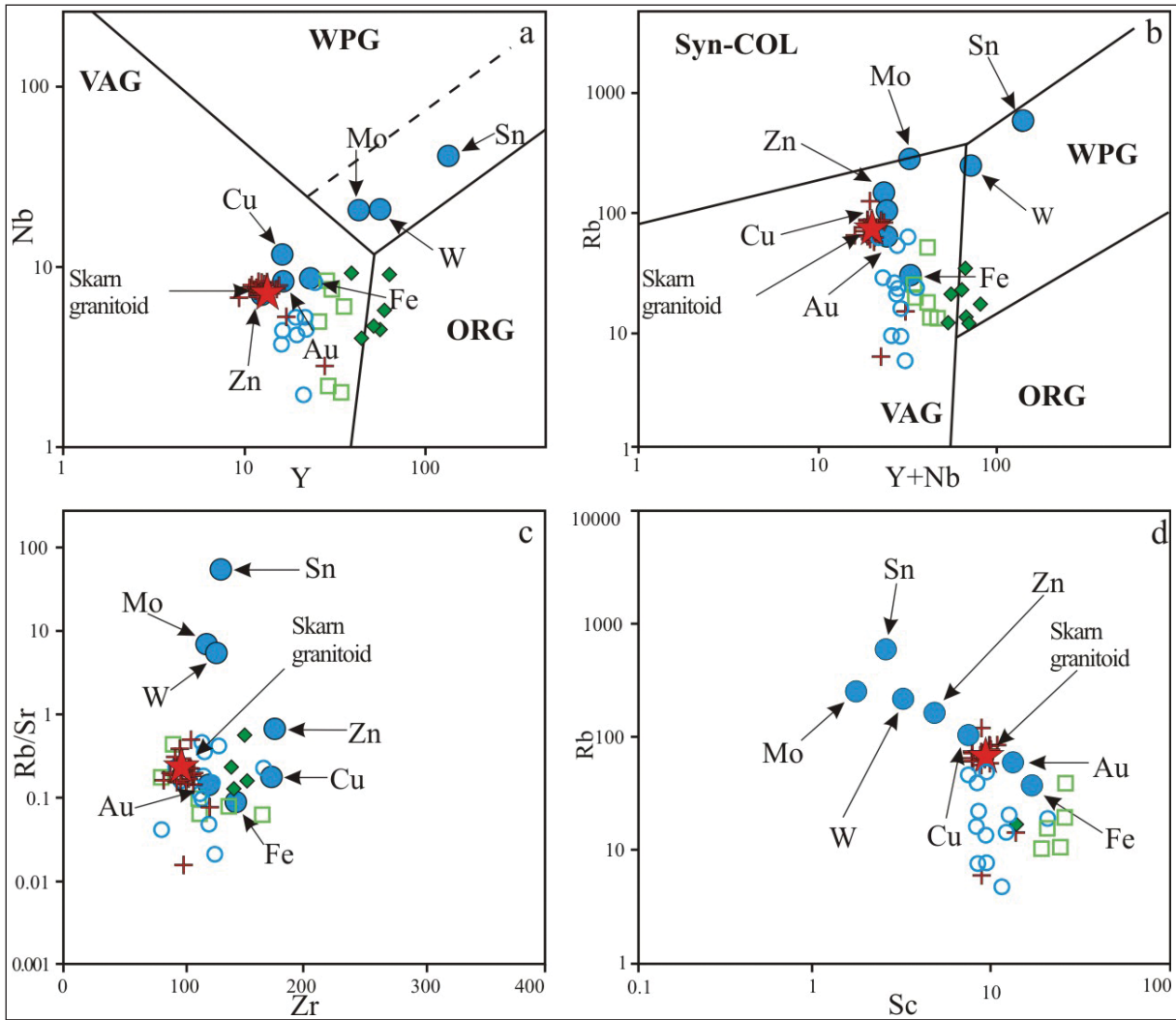


Figure 10- a, b) Distribution pattern of the skarn zone and the Dağbaşı granitoid samples plotted together on the Nb–Y and Rb–(Nb–Y) trace element diagrams used in defining tectonic settings (Pearce et al., 1984) and comparison of these with the granitoids causing different types of skarns (WPG: within plate granitoids, ORG: ocean ridge granitoids, VAG: volcanic arc granitoids, syn-COL: collision granitoids; dashed lines show the upper limit of the ORG anomaly values); c, d) distribution pattern of the Dağbaşı Granitoid samples on the Zr–Rb/Sr and Sc–Rb diagrams and comparison of them with the compositions of plutonic rocks with different skarn types (Meinert, 1995; symbols same as in figure 8c).

composition  $And_{0-8.81}Grs_{59.69-78.65}Prs_{21.35-38.11}$ , whereas late garnets are of andradite type with a composition of  $And_{74.67-100}Grs_{0-22.81}Prs_{0-2.52}$ . Accordingly, early and late stage garnets from the İpekçili locations have similarities with the dominant grossular type at the early stage ( $And_{0-8.81}Grs_{55.67-66.53}Prs_{32.40-38.00}$ ) and dominant andradite type at the late stage ( $And_{75.71-99.96}Grs_{0-21.80}Prs_{0-4.41}$ ).

It is possible to show the ideal stoichiometric compositions of the minerals by plotting their analyses on triangular diagrams as end members (Meinert, 1992). The chemical compositions of early and late stage garnets from Köprüüstü and İpekçili locations have

been plotted on a (pyrope+spessartine+almandine)–grossular–andradite triangular diagram separately (Figure 11a). According to this, late stage garnets have high andradite and low grossular contents. On the other hand, both grossular and almandine contents are high in the early stage garnets.

Microscopic studies show that garnets in the limestones have zonation from core to rim. Mineral chemistry analyses performed on these zoned crystals from core to rim confirm that there are some variations in the element concentrations which reflect the changes in the chemistry of solutions. In both Köprüüstü and İpekçili locations, the  $Al_2O_3$  content of the early

Table 2- EPMA analyses representing early and late stage garnets from the Köprüüstü and İpekçili skarns (bdl: below detection limit).

Sample No	E27	E27	E27	E27	E27	E71	E71	E71	E71	E71	49	49	49	49	49	KL2	KL2	KL2	KL2	KL2	KL2	
Analyses No	1	2	3	4	5	7	8	9	10	11	1	2	3	4	5	12	13	14	15	16	16	
SiO <sub>2</sub>	36.58	37.25	37.36	37.23	37.23	34.06	34.54	33.99	34.17	33.96	37.49	37.78	38.11	37.61	38.19	34.94	34.93	34.91	35.60	35.06	35.06	
TiO <sub>2</sub>	bdl	0.11	0.11	0.10	0.17	bdl	bdl	0.01	bdl	bdl	0.05	0.03	0.20	0.11	0.12	bdl	bdl	0.02	bdl	bdl	bdl	
Al <sub>2</sub> O <sub>3</sub>	20.66	23.01	23.35	23.22	23.15	0.72	0.95	0.34	0.15	1.48	20.47	21.23	20.79	20.95	23.56	0.41	0.84	1.74	0.38	1.05	1.05	
Fe <sub>2</sub> O <sub>3</sub>	16.30	13.46	12.95	13.02	13.30	30.15	29.50	30.38	30.08	28.17	17.56	16.24	16.83	16.34	13.57	31.40	30.56	29.82	31.45	30.54	30.54	
MnO	0.06	0.06	0.01	bdl	0.04	0.43	0.62	0.40	0.35	0.48	0.37	0.17	0.12	0.32	0.23	0.58	0.68	0.83	1.43	0.61	0.61	
MgO	0.01	0.05	0.04	0.06	0.05	bdl	0.01	bdl	bdl	bdl	0.03	0.02	0.46	0.54	0.05	0.01	0.01	0.01	bdl	bdl	bdl	
CaO	23.17	23.51	23.62	23.55	23.55	31.76	31.66	31.58	31.44	30.79	22.96	22.93	23.25	22.74	23.71	32.81	32.12	32.34	32.51	32.88	32.88	
Na <sub>2</sub> O	0.02	bdl	0.01	bdl	bdl	0.01	0.02	0.01	bdl	bdl	0.01	bdl	bdl	bdl	0.01	0.01	bdl	bdl	0.02	bdl	bdl	
K <sub>2</sub> O	bdl	bdl	0.01	bdl	bdl	bdl	bdl	bdl	0.01	bdl	bdl	bdl	0.15	0.20	bdl	bdl	bdl	0.01	0.02	bdl	bdl	
Total	96.80	97.45	97.46	97.18	97.49	97.12	97.30	96.71	96.21	94.88	98.93	98.40	99.89	98.82	99.43	100.16	99.14	99.69	101.40	100.15	100.15	
Si	2.954	2.920	2.913	2.915	2.913	2.953	2.979	2.962	3.024	2.992	2.970	2.990	2.979	3.017	2.927	2.944	2.976	2.940	2.964	2.944	2.944	
Al iv	0.046	0.080	0.087	0.085	0.087	0.047	0.021	0.037	-	0.008	0.030	0.010	0.021	-	0.073	0.044	0.024	0.060	0.036	0.056	0.056	
Al vi	1.925	2.062	2.080	2.077	2.066	0.031	0.082	-	0.016	0.156	1.888	1.973	1.900	1.956	2.073	-	0.067	0.125	0.003	0.056	0.056	
Ti	-	-	0.007	0.006	0.010	-	-	0.006	-	-	0.003	0.002	0.012	0.006	0.007	-	-	0.001	-	-	-	-
Fe <sup>3+</sup>	0.067	-	-	-	-	1.634	1.592	1.657	1.671	1.535	0.096	0.023	0.078	0.060	-	1.668	1.623	1.561	1.655	1.615	1.615	
Fe <sup>2+</sup>	1.035	0.973	0.963	0.962	0.969	0.552	0.536	0.557	0.414	0.541	1.067	1.053	1.022	0.850	0.974	0.544	0.503	0.539	0.535	0.530	0.530	
Mn	0.004	0.004	0.001	-	0.002	0.031	0.045	0.030	0.027	0.036	0.025	0.012	0.008	0.022	0.015	0.041	0.049	0.059	0.101	0.043	0.043	
Mg	0.001	0.006	0.005	0.007	0.006	-	0.001	-	-	-	0.003	0.002	0.053	0.065	0.005	0.002	0.001	0.002	-	-	-	
Ca	2.005	1.975	1.974	1.976	1.974	2.950	2.926	2.949	2.981	2.907	1.949	1.945	1.947	1.954	1.947	2.962	2.933	2.918	2.900	2.959	2.959	
Total	8.036	8.026	8.029	8.027	8.027	8.199	8.183	8.194	8.133	8.174	8.031	8.008	8.019	7.931	8.021	8.205	8.176	8.204	8.193	8.203	8.203	
Prop	0	0.2	0.2	0.2	0.2	0	0	0	0	0	0.1	0.1	1.8	2.2	0.2	0.1	0.1	0.1	0	0	0	
Spessartine	0.1	0.1	0	0	0.1	1.2	1.8	1.1	0.9	1.4	0.8	0.4	0.3	0.8	0.5	1.6	1.9	2.3	2.2	1.7	1.7	
Almandine	32.0	32.1	32.0	32.0	31.9	0	0	0	0	0	33.4	34.5	32.6	29.4	32.8	0	0	0	0	0	0	
Andradite	3.4	-	-	-	-	95.7	94.3	98.0	99.1	90.9	4.9	1.1	3.9	3.1	-	97.6	95.0	90.0	97.8	93.9	93.9	
Grossular	64.5	67.6	67.8	67.8	67.8	3.1	3.9	0.9	0.0	7.7	60.8	63.9	61.4	64.5	66.5	0.7	3.0	7.6	-	4.4	4.4	

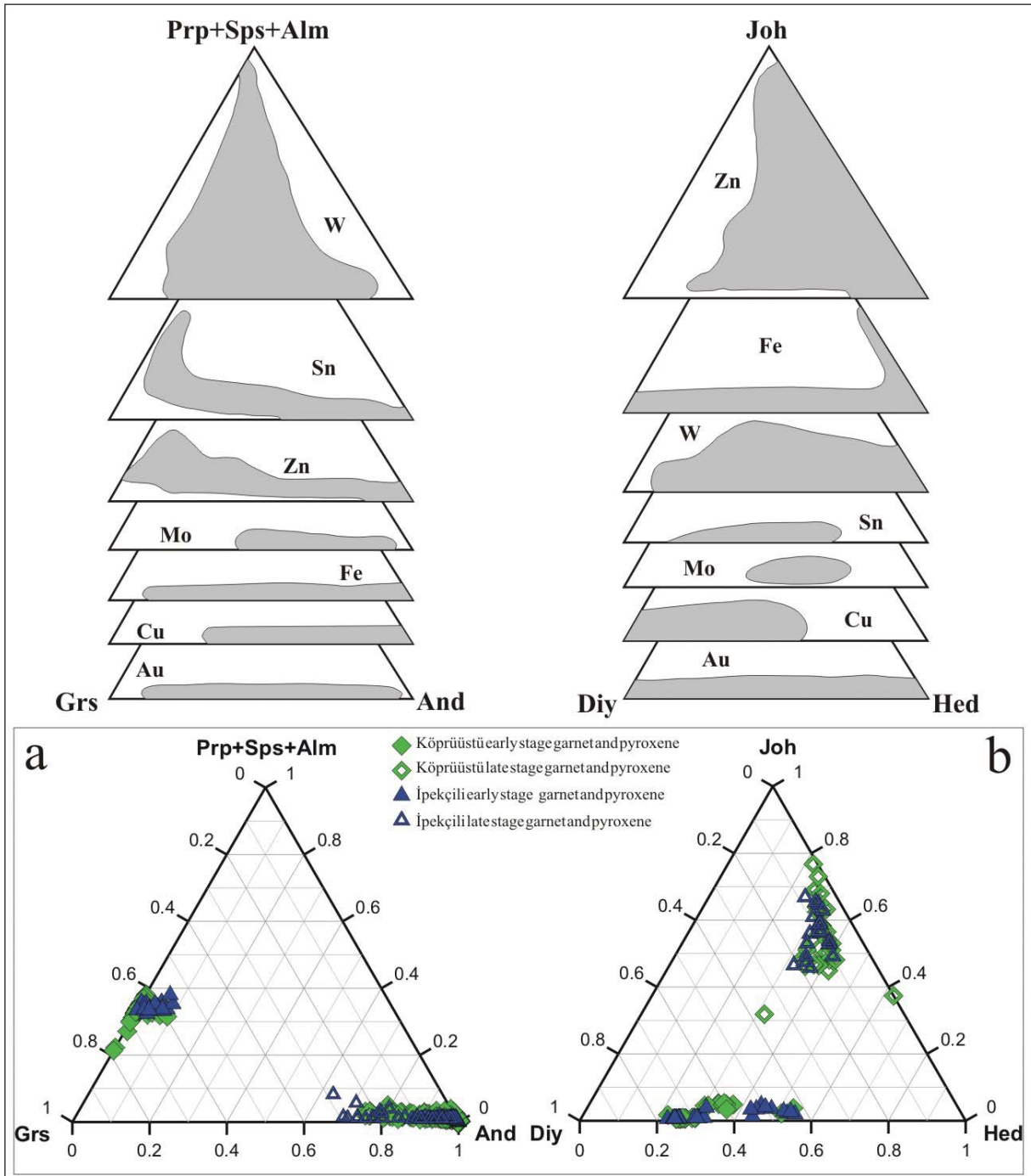


Figure 11- Skarn type classifications based on the garnet and pyroxene compositions (Einaudi et al., 1981; Meinert, 1983, 1982): a, b) compositional variations in the early- and late-stage garnets and pyroxenes in the Köprüüstü and İpekçili skarns (Prp: pyrope, Sps: spessartine, Alm: almandine, Grs: grossular, And: andradite; Joh: johannsenite, Diy: diopside, Hed: hedenbergite).

stage grossular-type garnet ( $X_{\text{Grs}}$ : 0.60–0.79 and  $X_{\text{Grs}}$ : 0.56–0.67, respectively) decreases in zoned crystals from core to rim while FeO increases (Figure 12). This zonation indicates that the garnet composition changes from grossular type  $\text{Ca}_3\text{Al}_2(\text{SiO}_4)_3$  to andradite  $\text{Ca}_3\text{Fe}_2(\text{SiO}_4)_3$ .

Profile analyses of garnet with andradite ( $X_{\text{And}}$ : 0.75–1) composition shows zonation from core to rim (Figure 13). In these minerals, the  $\text{Al}_2\text{O}_3$  contents decrease while FeO contents increase from core to rim. According to this, in garnets with andradite composition, the And/Grs ratio shows a greater increase from core to rim.

4.3.2. Pyroxene

In the Köprüüstü and İpekçili locations, pyroxenes have been classified into two groups, representing early and late stage developments. The results of the pyroxene analyses are given in table 3. According to these analyses, the pyroxene compositions are given in the hedenbergite–diopside–johannsenite triangular diagram (Figure 11b). The composition of early

stage pyroxenes in the Köprüüstü location has been calculated as  $\text{Hed}_{24.59-29.57}\text{Diy}_{69.65-74.76}\text{Joh}_{0.6-0.88}$ , while the late pyroxene composition is  $\text{Hed}_{22.17-62.63}\text{Diy}_{0-36.2}\text{Joh}_{31.86-76.69}$ . In the İpekçili location, the composition of early stage pyroxenes is  $\text{Hed}_{22.44-31.81}\text{Diy}_{67.3-76.99}\text{Joh}_{0.52-0.88}$  and the late stage pyroxenes have a composition of  $\text{Hed}_{24.95-40.97}\text{Diy}_{5.62-21.25}\text{Joh}_{45.76-66.93}$ . In both locations, the early stage pyroxenes have compositions between hedenbergite–diopside. In the late stage pyroxene, there is an increase in the johannsenite content (Figure 11b). In the late stage pyroxenes, the increase in johannsenite content is related to the increase in  $\text{Mn}^{2+}$ . Since the increase in manganese would increase the Mn/Fe ratio, in the late stage pyroxenes containing johannsenite, this ratio would be quite high, reaching 0.78–3.42. On the other hand, in the early stage pyroxenes, this ratio ranges between 0.02 and 0.15.

To study skarn types and classifications, the compositions of garnets and pyroxenes have been plotted on the triangular diagrams proposed by Einaudi et al. (1981) and Meinert (1983, 1992). According to these diagrams, early stage garnets with high grossular

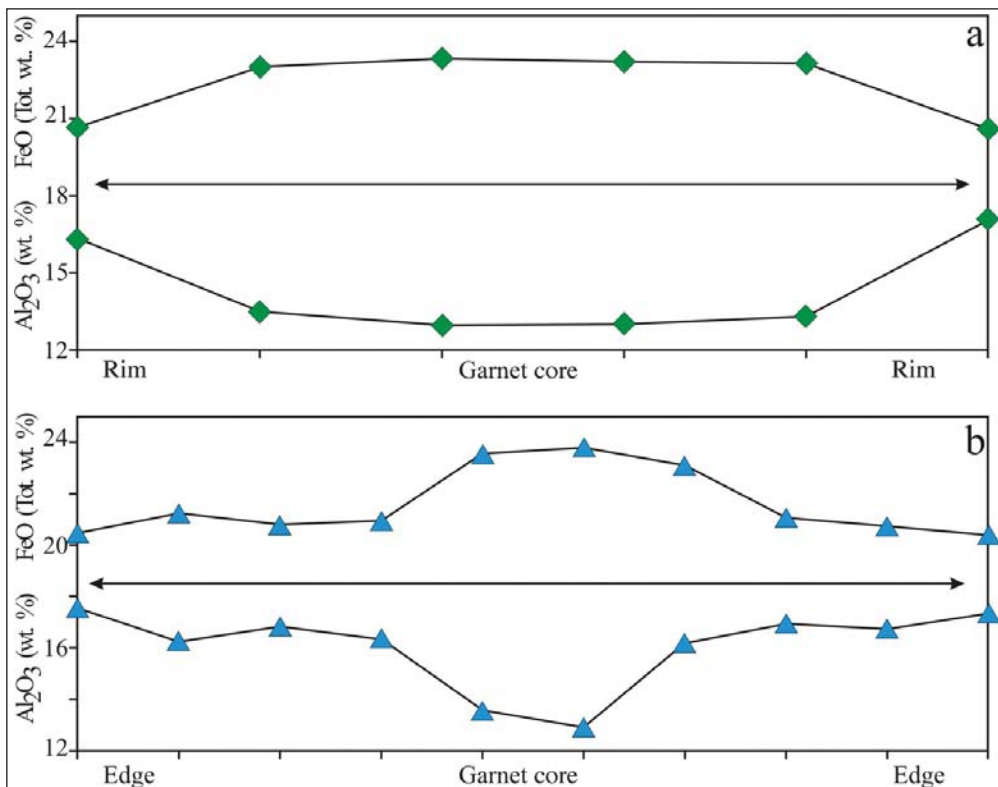


Figure 12- FeO and  $\text{Al}_2\text{O}_3$  variations along the zoned garnet crystals, from core to rim, in the early stage garnet (grossular type) of the Köprüüstü (a) and İpekçili (b) locations.

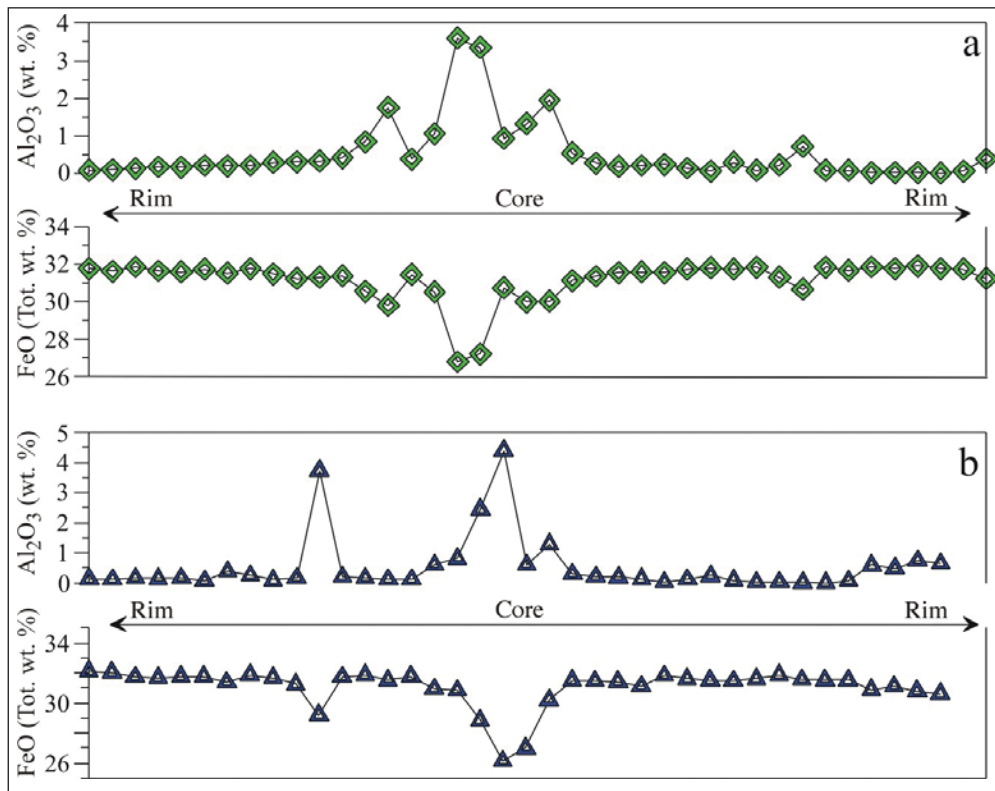


Figure 13- FeO and Al<sub>2</sub>O<sub>3</sub> variations along the zoned garnet crystals, from core to rim, in the late stage garnets (andradite type) of the Köprüüstü (a) and İpekçili (b) locations.

and almandine contents do not have any relation with the skarn types but late stage garnets with high andradite contents have compositions similar to those of the Fe-, Cu-, and Zn-type skarns. On the other hand, early stage pyroxenes with compositions changing between diopside and hedenbergite have similar compositions to the Au, Cu, Sn, and W skarn types. But the late stage pyroxenes with high johannsenite contents are in close characteristic association with Zn-type skarns (Figure 11a, b).

#### 4.4. Mineral Chemistry of Sulfurs

In the Kükürtlü and Dere Mahalle districts in the Dağbaşı area, magnetite and hematite are the main skarn ore minerals. There are some micron-sized pyrite and chalcopyrite inclusions in the magnetites and hematites in some of the polished sections of the samples from these locations (Figure 6o). On the other hand, in the İpekçili and Köprüüstü skarn locations, there is a significant amount of sulfur minerals in addition to the magnetites and hematites. The major and trace element contents of sulfur minerals of pyrrhotite, pyrite, sphalerite, and galena are given in tables 4 and 5.

Pyrrhotite is not a common mineral in other locations but it is a common mineral in the İpekçili ores. In the chemical analyses of the pyrrhotites, some high concentrations of elements are as follows: Pb 1.30%, As 0.39%, Cd 0.12%, and Ag 0.13%. According to the analyses, pyrrhotites show up to 10% deviation from the stoichiometric composition (FeS), and the chemical formula is calculated as Fe<sub>(1-0.1)</sub>S<sub>(1+0.1)</sub>. In the pyrrhotite analyses carried out along the profile from core to the rim, the Fe content decreases while the S content increases (Figures 14a, b). Therefore, pyrrhotites are close to the stoichiometric composition in the core, but towards the rim they show deviation from the stoichiometric composition depending on decreases in Fe.

Pyrites accompany pyrrhotite, chalcopyrite, and sphalerite in the İpekçili ore, while they accompany chalcopyrite, sphalerite, and galena in the Köprüüstü ore. According to the mineral chemistry analyses, pyrites include up to 4.31 wt% Pb, 1.4 wt% Zn, 1.29 wt% Cu, 0.78 wt% As, and 0.25 wt% Cd. Apart from these, four out of 46 analyses contain Co, varying between 0.06 and 0.47 wt%, and Ni is always below detection limit.



Table 4- Results of the representative mineral chemistry analyses of the pyrrhotite, pyrite and chalcopyrite.

Sample No	Pyrrhotite										Pyrite										Chalcopyrite									
	İpekcilli					İpekcilli					Köprüüstü					İpekcilli					Köprüüstü									
	D6-13	D6-59	D6-59-8	D5-19	D5-22	D5-24	D6-2-1	D6-2-2	D6-2-8	K10-8	K10-9	K10-11	KL1-20	D6-11	D6-22	K11-13	K11-13-2	K10-11	K10-16	K10-29										
Fe	57.70	60.16	59.55	64.22	63.45	63.46	45.82	45.44	45.21	45.66	46.80	46.33	46.06	30.16	30.50	30.18	30.31	29.65	29.61	29.40										
Pb	0.82	bdl	bdl	bdl	0.18	bdl	1.30	0.82	bdl	bdl	0.34	0.64	bdl	1.37	1.54	0.68	1.30	0.51	0.74	bdl										
As	bdl	bdl	bdl	bdl	bdl	0.13	0.28	0.36	0.29	bdl	bdl	0.08	0.28	bdl	0.06	0.22	0.24	0.35	bdl	0.30										
Zn	bdl	bdl	bdl	bdl	bdl	bdl	bdl	bdl	bdl	1.42	0.94	0.73	bdl	bdl	bdl	0.07	bdl	0.40	1.35	1.73										
Cd	0.07	bdl	bdl	bdl	0.08	0.07	0.10	bdl	bdl	bdl	0.17	0.15	bdl	bdl	bdl	0.08	bdl	bdl	bdl	0.15										
Ag	bdl	0.10	bdl	0.11	bdl	bdl	bdl	bdl	0.07	bdl	0.15	0.08	bdl	0.07	bdl	bdl	bdl	bdl	bdl	bdl										
Cu	0.07	0.06	bdl	bdl	bdl	bdl	bdl	bdl	bdl	0.13	0.08	0.05	0.44	32.89	32.53	34.12	33.94	34.67	34.10	33.61										
Co	bdl	bdl	bdl	bdl	bdl	bdl	bdl	bdl	bdl	0.47	bdl	0.06	0.34	bdl	bdl	bdl	bdl	bdl	bdl	bdl										
S	40.08	39.64	39.60	36.93	36.81	37.38	53.23	54.01	54.03	52.13	52.51	52.30	53.39	34.37	33.99	34.81	34.56	33.94	34.97	35.15										
Total	98.59	99.71	99.41	100.99	100.77	100.44	100.54	100.45	99.45	99.81	100.20	100.37	99.37	98.99	98.37	100.09	100.41	99.02	99.99	98.84										
Fe	0.903	0.930	0.925	0.998	0.994	0.986	0.988	0.974	0.972	0.991	1.007	1.004	0.987	1.011	1.027	0.996	1.003	0.989	0.972	0.964										
Pb	0.003	-	0.003	-	0.001	-	0.008	0.005	-	-	0.002	0.004	0.004	0.012	0.014	0.006	0.012	0.005	0.007	-										
As	-	-	-	-	-	0.001	0.005	0.006	0.005	-	-	0.001	0.004	-	0.001	0.005	0.006	0.009	-	0.007										
Zn	-	-	-	-	-	-	-	-	-	0.026	0.017	0.014	-	-	-	0.002	-	0.012	0.038	0.048										
Cd	0.001	-	-	-	0.001	0.001	0.001	-	-	-	0.002	0.002	-	-	-	0.001	-	-	-	0.002										
Ag	-	0.001	-	0.001	-	-	-	-	0.001	-	0.002	0.001	-	0.001	-	-	-	-	-	-										
Cu	0.001	0.001	-	-	-	-	-	-	-	0.003	0.001	0.001	0.008	0.969	0.963	0.989	0.987	1.016	0.984	0.969										
Co	-	-	-	-	-	-	-	-	-	0.010	-	0.001	0.007	-	-	-	-	-	-	-										
S	1.092	1.068	1.071	1.000	1.004	1.011	1.998	2.015	2.022	1.970	1.968	1.973	1.993	2.006	1.993	2.000	1.991	1.970	2.000	2.008										
Total	2.000	2.000	2.000	2.000	2.000	2.000	3.000	3.000	3.000	3.000	3.000	3.000	3.000	4.000	4.000	4.000	4.000	4.000	4.000	4.000										

Table 5-. Results of the representative mineral chemistry analyses.

Sample No	Sphalerite												Galena									
	İpekközü						Köprüüstü						Köprüüstü									
	K11-5	K11-6	K11-9	K11-13	K11-14	K10-16	K10-17	K10-18	K10-20	K10-22	K10-24	K10-3	K10-7	K10-8	K10-10	K10-12	K10-3-9	K10-3-10				
Fe	2.42	2.81	3.16	4.64	3.70	4.76	2.19	2.73	2.75	3.08	2.58	bdl	0.15	0.18	0.42	0.23	0.42	0.49				
Pb	bdl	0.11	0.32	0.28	0.92	bdl	0.37	2.03	bdl	1.01	bdl	82.89	83.15	82.11	82.74	83.52	81.23	82.76				
As	bdl	0.12	bdl	bdl	0.22	bdl	bdl	bdl	0.26	bdl	bdl	bdl	bdl	bdl	bdl	bdl	bdl	bdl				
Zn	65.25	64.95	63.13	59.95	62.74	59.19	65.57	64.30	64.03	65.77	0.18	0.55	0.19	0.19	bdl	0.35	0.91	0.47				
Cd	0.45	0.41	0.18	0.08	0.39	0.28	0.19	0.11	0.13	0.23	0.32	bdl	bdl	bdl	bdl	0.06	0.13	0.22				
Ag	bdl	0.06	bdl	bdl	0.15	bdl	bdl	bdl	0.13	bdl	0.06	1.39	1.22	1.28	1.37	1.30	1.43	1.26				
Cu	0.53	0.36	1.23	2.07	0.69	2.67	0.36	0.19	0.43	0.62	0.28	0.05	0.26	0.83	0.10	0.37	1.14	0.72				
Co	bdl	bdl	bdl	0.09	bdl	bdl	0.05	bdl	bdl	bdl	0.05	bdl	0.06	bdl	bdl	bdl	bdl	bdl				
S	30.96	30.85	32.35	31.45	31.61	32.59	31.54	31.77	31.58	31.45	31.83	13.88	13.59	13.41	13.42	13.28	13.71	14.23				
Total	99.41	99.62	100.15	98.55	100.65	99.42	100.12	100.72	100.01	100.14	100.49	98.41	98.98	98.04	98.11	99.12	99.02	100.18				
Fe	0.043	0.050	0.055	0.082	0.065	0.083	0.039	0.048	0.048	0.054	0.045	-	0.006	0.008	0.018	0.010	0.017	0.020				
Pb	-	0.001	0.002	0.001	0.004	-	0.002	0.010	-	0.005	-	0.942	0.941	0.937	0.950	0.954	0.897	0.903				
As	-	0.002	-	-	0.003	-	-	-	0.001	0.003	-	-	-	-	-	-	-	-				
Zn	0.988	0.984	0.939	0.909	0.942	0.882	0.985	0.965	0.976	0.962	0.979	0.006	0.020	0.007	-	0.013	0.032	0.016				
Cd	0.004	0.004	0.002	0.001	0.003	0.002	0.002	0.001	0.001	0.002	0.003	-	-	-	-	0.001	0.003	0.004				
Ag	-	0.001	-	-	0.001	-	-	-	0.001	-	0.001	0.030	0.027	0.028	0.030	0.029	0.030	0.026				
Cu	0.008	0.006	0.019	0.032	0.011	0.041	0.006	0.003	0.007	0.010	0.004	0.002	0.009	0.031	0.004	0.014	0.041	0.026				
Co	-	-	-	0.003	-	-	0.001	-	-	-	0.001	-	0.002	-	-	-	-	-				
S	0.956	0.953	0.982	0.973	0.969	0.991	0.966	0.972	0.965	0.963	0.967	1.019	0.994	0.989	0.996	0.980	0.978	1.003				
Total	2.000	2.000	2.000	2.000	2.000	2.000	2.000	2.000	2.000	2.000	2.000	2.000	2.000	2.000	2.000	2.000	2.000	2.000				

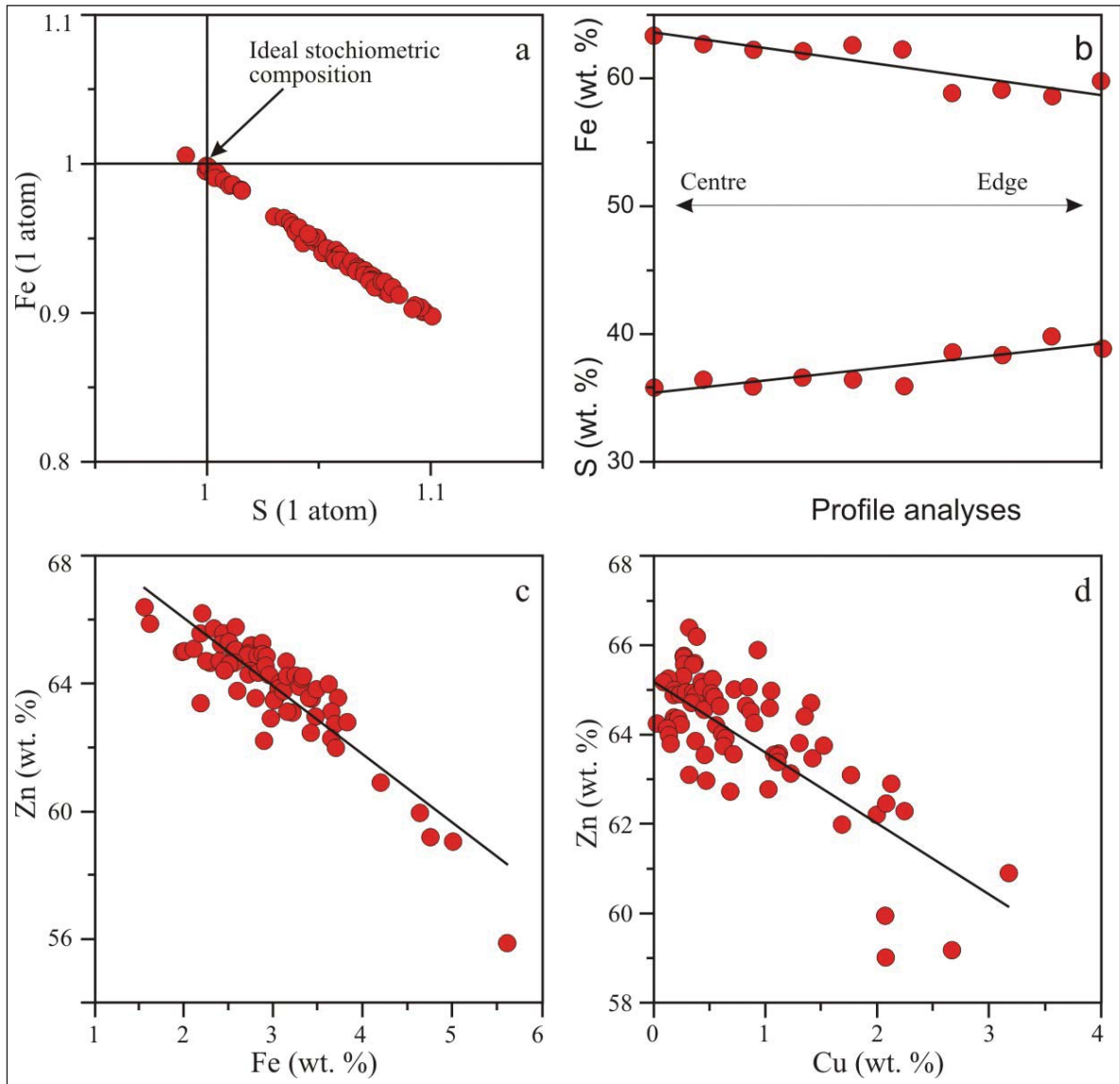


Figure 14- a) Stoichiometric compositional changes of the pyrrhotites in the İpekçili ore; b) Fe versus S variations on the profile analyses of pyrrhotites; c, d) correlations showing element substitution in sphalerites of the Köprüüstü ore.

Chalcopyrites in both İpekçili and Köprüüstü locations contain up to 1.82 wt% Pb, 2.6 wt% Zn, and 0.47 wt% As. The general formula of these chalcopyrites has been calculated as  $\text{Fe}_{0.96-1.05}\text{Cu}_{0.97-1.04}\text{S}_{1.95-2.02}$ . No differences were detected between different locations in terms of trace element concentrations.

Sphalerites always accompany to other sulfides in both locations but are more abundant in the Köprüüstü ore than in the İpekçili location. In the analyses of sphalerite, apart from the main element of Zn, higher concentrations of some other elements are 5.01 wt% Fe, 3.18 wt% Cu, 2.04 wt% Pb, and 0.45 wt% Cd. The

negative correlations between Fe and Zn and between Cu and Zn indicate elemental substitution between these elements (Figures 14c, d).

Galena is only present in the Köprüüstü location. It is always observed as inclusions in sphalerites, and modal abundances are less than 1% in the ore. The highest concentrations of some elements measured in galena are 1.43 wt% Ag, 1.14 wt% Cu, 0.91 wt% Zn, and 0.49 wt% Fe. On the basis of mineral chemistry analyses, the formula of galena is calculated as  $\text{Pb}_{(0.94-0.95)}\text{S}_{(0.98-1.02)}$ . Apart from Ag, the concentrations of the other elements show variations between the detection limits and the higher concentrations given above. On

the other hand, nine separate galena analyses show that the Ag contents are always higher than 1 wt%, showing very close variations of between 1.18 and 1.43 wt%. This suggests that galena minerals may have silver potential in the study area.

## 5. Discussion and Results

### 5.1. Host Rocks' Relations and Skarn Mineralogy

The Dağbaşı skarn ores have developed as an exoskarn type along the nearest border of the Upper Cretaceous Dağbaşı Granitoid and block- and lens-shaped limestones of Berdiga formation which are located in the Liassic volcanics. In the field studies, neither contact between limestones and granitoid nor the development of skarn minerals in the granitoid has been observed. Since skarn-type deposits develop with metasomatic processes between granitoid and limestone, the absence of a contact relationship makes it difficult to explain the skarns in the region. However, although no contact relations were found in the field, as marked in the cross-sections (Figure 3), it is quite possible to claim that the granitoid and limestones may have contact below the surface. In this case, hydrothermal solutions interacting with the limestones along the underground contact reached the surface by spreading through the weak zones of the limestones. According to this explanation, the main skarn contact and ore zones are below the surface. The presence of numerous old adits and mine waste around them supports the idea that the main ore zone is below the surface.

The prograde stage is represented by garnet and pyroxene occurrences in the field, but in detail it is subdivided into early and late stages. The early prograde stage is represented by garnets and pyroxenes in the limestones forming massive, rhythmically banded, granular, and nodular textures. Garnet and pyroxene veins developed along the fractures in the limestones are considered to be the products of the late-prograde stage. Mineral chemistry analyses have also shown that these garnets and pyroxenes from both stages have different compositions. On the other hand, tremolite-actinolite, epidote, quartz, and calcites are products of the retrograde stage. The presence of magnetites and hematites in the growth zones in the garnets may indicate that ore mineralizations started in the late prograde stage, but the main ore mineralization developed in the retrograde stage. In addition to the fracture-filling-type ore veins in the limestones and

volcanic rocks, the presence of banded ore along the limestone layers indicates that oxide and sulfide ore mineralization developed in the retrograde stage.

### 5.2. Skarn Types and Formation Conditions

Chemical analyses of the garnets from the Köprüüstü and İpekçili locations indicate that garnet compositions change between grossular and andradite. Early stage garnets have higher grossular compositions and have a total of up to 38% pyrope+spessartine+almandine in the chemical formula ( $\text{And}_{0-8.81}\text{Grs}_{55.67-78.65}\text{Prs}_{32.40-38.00}$ ). According to Einaudi et al. (1981), reducing skarns are characteristic with their low andradite ( $\text{Fe}^{3+}$ ) and high spessartine ( $\text{Mn}^{2+}$ ) and almandine ( $\text{Fe}^{2+}$ ) contents. According to this explanation, the high grossular and almandine contents of early prograde stage garnets indicate the reducing skarn type. On the other hand, late stage garnets with higher andradite contents indicate oxidized skarn types (Jamtveit, 1991; Jamtveit and Hervig, 1994; Clechenko and Valley, 2003; Ciobanu and Cook, 2004; Meinert et al., 2005; Orhan and Mutlu, 2009). Einaudi (1981) also suggests that  $\text{Fe}^{3+}$ -rich garnets (andradite) are quite common in oxidized skarns and also suggest that andradite-rich garnets may be an indication of the shallow emplacement of granitoids.

Taking into account the explanation given above, grossular-type early stage garnets and andradite-type late stage garnets show a transition from reduced to oxidized skarn. These type changes in the oxidation degree of skarn have been explained by the fracturing of overlying rocks along the skarn contact due to the increasing hydraulic pressure (Yardley and Lioyd, 1995; Dipple and Gerdes, 1998; Clechenko and Valley, 2003; Meinert et al., 2005). According to this, increased permeability and porosity of the host rocks allow the circulation of meteoric water through the skarn environments. Similar findings were also reported by Orhan (2017), who noted that the garnet composition of the early stage changes from grossular type to the andradite one in the Kozbudaklar skarn. In this study, the transition from grossular to andradite has also been explained by the introduction of meteoric water into the skarn zone.

In this study, analyses conducted along the profile line of the grossular- and andradite-type zoned garnet crystals showed increases in the And/Grs ratios from core to rim. In similar studies, researchers indicate that zoned garnet crystals can be used to understand the formation condition of skarns (Collins, 1977;

Newberry, 1983; Abu el Enen et al., 2004). These researchers have argued that the zoning from the centre to the rim reflects the evolution of fluids. According to this explanation, increased And/Grs ratios in the zoned garnets are related to the increase in the degree of oxidation  $f(O_2)$  of the skarns. In this study, the increase of the And/Grs ratio in the skarn minerals from the centre towards the rim could be explained by the increase in the oxidation rate.

There is a systematic relation between the element content of the pyroxene and the metal content of the skarn-type deposits (Burt, 1972; Einaudi et al., 1981; Newberry, 1991; Nakona et al., 1994; Nakona, 1998). Depending upon the skarn type, the Mg, Mn, and Fe contents of pyroxenes show variations (Einaudi and Burt, 1982). According to this explanation, Mn-containing pyroxenes (johannsenite) represent Zn-type skarns, while diopside- and hedenbergite-containing pyroxenes represent Cu–Fe-type skarns. Plotting the element contents of pyroxenes on the triangular diagrams showed that late stage pyroxenes from the Köprüüstü and İpekçili locations with their high Mn contents fall into the Zn-type skarn area (Figure 11b). On the other hand, early stage pyroxenes from these two locations fall into the Cu–Fe-type skarn area (Figure 11b).

Studies on skarn-type deposits showed that in addition to the Mn content of pyroxenes, Mn/Fe ratios could also be used in the classification of skarn-type deposits (Nakano et al., 1994; Nakano, 1998). In these studies, it is suggested that the Mn/Fe ratios of pyroxenes are  $< 0.1$  for Cu–Fe skarns,  $0.1-0.2$  for W-type skarns, and  $> 0.2$  for Pb–Zn-type skarns. In this study, the Mn/Fe ratios of early stage pyroxenes from the Köprüüstü and İpekçili locations show variation between 0.02 and 0.15, while late stage pyroxenes show variation between 0.78 and 3.42. Although the calculated Mn/Fe ratios of early stage pyroxenes show a little deviation from the value of 0.1, the data are mostly compatible for Cu–Fe-type skarns. On the other hand, Mn/Fe ratios ranging between 0.78 and 3.42 are characteristic for Zn-type skarns. The presence of sphalerite in the skarn paragenesis supports this approach.

### 5.3. Granitoid Geochemistry and Its Relation to Skarn Types

The compositions of magmatic rocks and their relations with skarn types and metal contents have

been studied by a number of researchers (Kwak and White, 1982; Meinert, 1983, 1995; Newberry and Swanson, 1986; Meinert et al., 1991, 2005; Kuşçu et al., 2001; Öztürk et al., 2005). According to these studies, granitoids associated with skarns have calc-alkaline compositions (Figure 8b). The Mg contents are higher in the granitoids associated with Fe, Au, and Cu-type skarn than in those associated with W, Sn, and Mo-type skarn (Figure 8c). On the other hand, plutons related to the Fe, Au, and Cu skarns have lower  $K_2O$  contents than the granitoids associated with W, Sn, and Mo skarns (Figure 8d). From the point of view of aluminium saturation, skarn-related plutons mostly have metaluminous–peraluminous transitional composition, except for the Sn skarns, which have a peraluminous composition, indicating granitoids of sedimentary origin (S-type). In addition, Fe-type skarn-related granitoids have metaluminous composition, indicating magmatic plutons of island arc origin (I-type) (Figure 8e).

Dağbaşı Granitoid is divided into four different zones by Aydınçakır (2006), namely granodiorite, monzogranite, tonalite, and diorite. Due to the heterogeneous composition of Dağbaşı Granitoid, the geochemical characteristics of the granitoid along the skarn zones have also been studied and correlated with skarn-related granitoids elsewhere. While samples collected from the granitoid along the skarn zones have compositions between granodiorite and tonalite, samples from the other parts have tonalite composition (Figure 8a). Based on the major element contents, all of the granitoid samples have calc-alkaline composition. While the  $K_2O$  contents of the granitoid samples from the skarn zones point to Fe–Cu skarns, granitoid samples from the other parts do not have a connection with the skarn types. The MgO contents of the skarn-zone granitoids have close similarity with Fe–Cu skarns, while samples from the other parts have a resemblance with W, Sn, and Mo skarns. In terms of the aluminium saturation, granitoids along the skarn zones have metaluminous–peraluminous transition, whereas granitoids from the other parts in general have peraluminous compositions.

On the basis of the tectonic setting and their various trace element contents, plutonic rocks have been classified in relation to the skarn types in previous studies (Meinert et al., 1991, 2005; Kuşçu et al., 2002; Öztürk et al., 2005). In those studies, Fe, Au, Cu, and Zn skarns were associated with volcanic arc granitoids, and Sn, W, and Mo skarns with within-

plate granitoids. In this study, analyses of the granitoid samples from the skarn zones have been plotted on the Nb–Y, Rb–Y+N trace element variation diagrams which were used for the determination of the tectonic setting of the granitoid. The result shows that they are of volcanic arc type (VAG) (Figures 10a, b). Comparing the trace element contents of the Dağbaşı granitoids with the others, Dağbaşı granitoids have compositions similar to those of the granitoids related to Fe–Cu–Zn-type skarns. Along with these, the Rb/Sr ratios and Rb contents of the Dağbaşı granitoids are considerably lower than those of the Sn-, Mo-, and W-related granitoids and resemble the Fe–Cu–Zn-producing granitoids in figure 10c and d.

In conclusion, major and trace element contents of Dağbaşı Granitoid along skarn zones have similar compositions with the granitoids producing Fe–Cu–Zn-type skarns. On the other hand, the other parts of the granitoid showing zonation with different mineralogy have quite different compositions. Accordingly, the presence of sulfide minerals (pyrrhotite, pyrite, chalcopyrite, sphalerite, and galena), in addition to oxide phase (magnetite and hematite), indicates that the skarn mineralogy is controlled by the geochemical properties of the granitoid.

### Acknowledgements

This study was supported by TÜBİTAK through project number 112Y331. Special thanks are due to Melanie Kaliwoda for providing the microprobe analyses for this study at the Mineralogy and Petrology Institute of Ludwig Maximilian University. Sincere thanks are offered to İbrahim Uysal for his help during the microprobe analyses. Raif Kandemir is thanked for his help during the microscopic studies. Great thanks are due to Emin Çiftçi and two anonymous reviewers whose comments improved the paper. Ali Dişli, Kadir Bayraktar, Mustafa Aksu and Mehdi İlhan are thanked for their assistance during the fieldwork and laboratory studies.

### References

- Abu El-Enen, M.M., Okrusch, M., Will, T.M. 2004. Contact metamorphism and metasomatism at a dolerite-limestone contact in the Gebel Yelleq area, Northern Sinai, Egypt. *Mineralogy and Petrology* 81, 135-164.
- Ağar, Ü. 1977. Demirözü (Bayburt) ve Köse (Kelkit) Bölgesinin Jeolojisi. Doktora Tezi, İÜ, Fen Fakültesi, İstanbul.
- Aslan, Z. 1991. Özdil (Yomra-Trabzon) Yöresinin Petrografisi Skarn Oluşukları ve Granat-Piroksen Ritmikleri. Yüksek Lisans Tezi, KTÜ Fen Bilimleri Enstitüsü, 72s, Trabzon.
- Aslaner, M. 1977. Türkiye bakır-kurşun-çinko yataklarının jeolojik ve bölgesel sınıflamasıyla plaka tektoniği yönünden incelenmesi. KTÜ, Yerbilimleri Fakültesi, Yayın No: 12, Trabzon.
- Aydınçakır, E. 2006. Dağbaşı (Araklı-Trabzon) granitoidi ve çevresinin petrografik, jeokimyasal ve petrolojik özelliklerinin incelenmesi. Yüksek Lisans Tezi, KTÜ, Fen Bilimleri Enstitüsü, 120s.
- Burt, D.M. 1972. Mineralogy and Geochemistry of Ca-Fe-Si Skarn Deposits. Ph.D. Thesis, Harvard University, 256p.
- Burt, D.M. 1982. Skarn deposits-historical bibliography through 1970. *Economic Geology* 77, 755-763.
- Ciobanu, C.L., Cook, N.J. 2004. Skarn texture and a case study: the Ocna de Fier-Dognecea orefield, Banat, Romania. *Ore Geology Reviews* 24, 315-370.
- Clechenko, C.C., Valley, J.W. 2003. Oscillatory zoning in garnet from the Willsboro Wollastonite Skarn, Adirondacks Mts, New York: a record of shallow hydrothermal processes preserved in granulite facies terrane. *Journal of Metamorphic Geology* 21, 771-784.
- Collins, B.I. 1977. Formation of scheelite-bearing and scheelite-barren skarns of Lost Creek, Pioneer Mountains, Montana. *Economic Geology* 72, 1505-1523.
- Çamur, M.Z., Tüysüz, N., Güven, İ.H., Arıkal, T., Er, M. 1994. Eastern Pontides Volcanism and Related Ore Deposits, International Volcanological Congress, IAVCEI, Ankara.
- Çiftçi, E. 2011. Sphalerite associated with pyrrhotite-chalcopyrite ore occurring in the Kotana Fe-skarn deposit (Giresun, NE Turkey): exolutions or replacement. *Turkish Journal of Earth Science* 20, 307-320.
- Çiftçi, E., Vıçıl, M. 2003. Kurtulmuş iron mineralization – an example to the skarn-type ore deposits from Eastern Pontides (Giresun, NE Turkey). *Geosound*, 26, 79-92.
- Debon, F., Le Fort, P. 1983. A chemical-mineralogical classification of common plutonic rocks and associations, *Trans. Roy. Soc., Edinburgh, Earth Science* 73, 135-149.
- Demir, Y., Uysal, I., Kandemir, R., Jauss, A. 2017. Geochemistry, fluid inclusion and stable isotope constraints (C and O) of the Sivrikaya Fe-skarn mineralization (Rize, NE Turkey). *Ore Geology Reviews* 91, 153-172.

- Dipple, G.M., Gerdes, M.L. 1998. Reaction-infiltration feedback and hydrodynamics at the skarn front. *Mineral. Assoc. Can., Short Course Series* 26, 71-97.
- Droop, G.T.R. 1987. A general equation for estimating Fe<sup>3+</sup> concentrations in ferromagnesian silicates and oxides from microprobe analyses, using stoichiometric criteria. *Mineralogical Magazine* 51, 431-435.
- Dunham, R.J. 1962. Classification of carbonate rocks according to depositional textures in W.E. Ham. (ed), *Classification of carbonate rocks*. American Association of Petroleum Geologist 1, 108-121.
- Einaudi, M.T., Meinert, L.D., Newberry, R.J. 1981. Skarn Deposits. *Economic Geology* 75, 317-391.
- Einaudi, M.T., Burt, D.M. 1982. A Special Issue Devoted to Skarn Deposits, Introduction-Terminology, Classification and Composition of Skarn Deposits. *Economic Geology* 77, 4, 745-754.
- Eren, M. 1983. Gümüşhane-Kale Arasının Jeolojisi ve Mikrofasiyes incelemeşi. Yüksek Lisans Tezi, KTÜ, Fen Bilimleri Enstitüsü, 197s, Trabzon.
- Folk, R.L. 1962. Spectral subdivision of limestone types in W.E. Ham. (Ed) *Classification of carbonate rocks*. AAPG Bulletin 1, 62-82.
- Gedikoğlu, A., Pelin, S., Özsayar, T. 1979. The main lines of the geotectonic evolution of the eastern pontides in mesozoik era. *Geocome* 1, 555-580.
- Gülibrahimoğlu, İ. 1986. Araklı güneyinin jeolojik etüt raporu, Maden Tetkik ve Arama Genel Müdürlüğü Rapor No: 2086, Ankara (unpublished).
- Güven, İ.H., Nalbantoğlu, A.K., Takaoğlu, S. 1998. 1/100.000 Ölçekli Açınsama Nitelikli Türkiye Jeoloji Harita Serisi, Maden Tetkik ve Arama Genel Müdürlüğü Yayını.
- Hasançebi, N. 1993. Dağbaşı (Araklı-Trabzon) granitoidine bağlı cevherleşmelerin incelenmesi. Yüksek Lisans Tezi, KTÜ Fen Bilimleri Enstitüsü, 65s, Trabzon.
- Irvine, T.N., Baragar, W.R.A. 1971. A guide to chemica classification of the common volcanic rocks. *Canadian Journal of Earth Science* 8, 523-548.
- Jamtveit, B. 1991. Oscillatory zonation patterns in hydrothermal grossular-andradite garnet: Nonlinear dynamics in regions of immiscibility. *American Mineralogist* 76, 1319-1327.
- Jamtveit, B., Hervig, R.L. 1994. Constraints on transport and kinetics in hydrothermal systems from zoned garnet. *Science* 263, 505-508.
- Kandemir, R. 2004. Gümüşhane Yakın Yörelerindeki Erken-Orta Jura Yaşlı Şenköy Formasyonu'nun Çökel Özellikleri ve Birikim Koşulları. Doktora Tezi, KTÜ Fen Bilimleri Enstitüsü, 274s, Trabzon.
- Kaygusuz, A. 1992. Dağbaşı (Araklı-Trabzon) ve Çevresinin Minerolojik ve Petrografik Olarak İncelenmesi. Yüksek Lisans Tezi, KTÜ Mimarlık-Mühendislik Fakültesi, 63s, Trabzon.
- Kaygusuz, A., Aydınçakır, E. 2011. U-Pb zircon SHRIMP ages, geochemical and Sr-Nd isotopic compositions of Cretaceous plutons in the eastern Pontides (NE Turkey): The Dağbaşı pluton. *Neues Jahrbuch für Mineralogie* 188, 211-233.
- Kesgin, Y. 1983. Bayburt (Gümüşhane) İlçesi, Akşar Köyü ve Güneybatısının Jeolojik İncelemeşi, Yüksek Lisans Tezi, KTÜ Fen Bilimleri Enstitüsü, 94s, Trabzon.
- Kırmacı, M.Z., Koch, R., Bucur, J.I. 1996. An Early Cretaceous section in the Kırcaova area (Berdiga Limestone, NE-Turkey) and its correlation with platform carbonates in W-Slovenia. *Facies* 34, 1-22.
- Kırmacı, M.Z., Yıldız, M., Kandemir, R., Eroğlu-Gümrük, T. 2018. Multistage dolomitization in late Jurassic-Early Cretaceous platform carbonates (Berdiga formation), Başoba Yayla (Trabzon), NE Turkey, Implication of the generation of magmatic arc on dolomitization. *Marine and Petroleum Geology* 89, 515-529.
- Koch, R., Bucur, I.I., Kırmacı, M.Z., Eren, M., Taslı, K. 2008. Upper jurassic and lower cretaceous carbonate rocks of the Berdiga limestone- sedimentation on an onbound platform with volcanic and episodic siliciclastic influx. *Biostratigraphy, facies and diagenesis (kırcaova, kale-gümüşhane area; NE-Turkey)*. *Neues Jahrb. für Geol. Palaontologie* 247, 23-61.
- Köprübaşı, N. 1992. Aşağı Harşit bölgesinin magmatik petrojenezi ve masif sülfütlere jeokimyasal hedef saptama uygulamaları, Doktora Tezi, KTÜ Fen Bilimleri Enstitüsü, Trabzon.
- Kurt, Y. 2014. Giresun, Bulancak Kirazören bölgesi skarn tipi demir yataklarının jeolojik ve jeokimyasal incelenmesi. Yüksek Lisans Tezi, İstanbul Üniversitesi, Fen Bilimleri Enstitüsü, 111s, İstanbul.
- Kuşçu, İ., Gençalioglu, G., Erler, A. 2001. Geochemical signatures of granitoids associated with skarn in central Anatolia. *International Geology Review* 43, 8, 722-735.

- Kuşçu, İ., Gençalioğlu, G., Meinert, D., Floyd, A. 2002. Tectonic setting and petrogenesis of the Çelebi granitoid, (Kırıkkale-Turkey) and comparison with skarn granitoids. *Journal of Geochemical Exploration* 76, 3, 175-194.
- Kwak, T.A.P., White, A.J.R. 1982. Contrasting W-Mo-Cu and W-Sn-F skarn types and related granitoids. *Mining Geology* 32, 4, 339-351.
- Maniar, P.D., Piccoli, P.M. 1989. Tectonic discrimination of granitoids. *Geological Society of Amerika Bulletin* 101, 635-643.
- Meinert, L.D. 1983. Variability of skarn deposits-guides to exploration, S.J. Boardman (Ed.), *Revolution in the earth sciences: Kendall-Hunt Publishing*, 301-316.
- Meinert, L.D. 1992. Skarn and skarn deposits. *Geoscience Canada* 19, 145-162.
- Meinert, L.D. 1995. Compositional variation of igneous rocks associated with skarn deposits, chemical evidence for a genetic connection between petrogenesis and mineralization. *Mineralogical Association of Canada, Short Course Series* 23, 401-418.
- Meinert, L.D., Brooks, J.W., Myers, G. L. 1991. Whole rock geochemistry and contrast among skarn types, in Bufa, R.H. and Coyner, A.R. (ed), *Geology and ore deposits of the Great Basin: Reno, Nevada, Geological Society of Nevada, Fieldtrip Guidebook Compendium 1*, 72-80.
- Meinert, L.D., Diple, G.M., Nicolescu, S. 2005. World skarn deposits, society of economic geologist. *Economic Geology 100th Anniversary Volume* 299-336.
- Nakano, T. 1998. Pyroxene Geochemistry as an Indicator for Skarn Metallogenesis in Japan, *Mineralized Intrusion-Related Skarn Systems*, D.R. Lentz. (Ed.), *Mineralogical Association of Canada, Short Course Series* 26, 147-167.
- Nakona, T., Yoshino, T., Shimazaki, H., Shimizu, M. 1994. Pyroxene Composition as an Indicator in the Classification of Skarn Deposits. *Economic Geology* 89, 1567-1580.
- Newberry, R.J. 1983. The formation of subcalcic garnet in scheelite-bearing skarns. *Canadian Mineralogist* 21, 529-544.
- Newberry, R.J. 1991. Scheelite-bearing skarns in the Sierra Nevada region, California: Contrast in zoning and mineral compositions and tests of infiltration metasomatism theory. In *skarns - Their Genesis and Metallogeny*, A. Barto- Kyriakidis (Ed.), *Theophrastus Publications, Atkens, Greece* 343-384.
- Newberry, R.J., Swanson, S.E. 1986. Scheelite skarn granitoids: An evaluation of the roles of magmatic source and process. *Ore Geology Reviews* 1, 57-81.
- Orhan, A. 2017. Evolution of the Mo-rich scheelite skarn mineralization at Kozbudaklar, Western Anatolia, Turkey: Evidence from mineral chemistry and fluid inclusions. *Ore Geology Reviews* 80, 141-165.
- Orhan, A., Mutlu, H. 2009. Susurluk (Balıkesir) skarn yatağının mineralojik ve petrografik Özellikleri. *Eskişehir, Osmangazi Üniversitesi Mühendislik Fakültesi Dergisi* 12, 2, 65-90.
- Oyman, T. 2010. Geochemistry, mineralogy and genesis of the Ayazmant Fe-Cu skarn deposit in Ayvalık, (Balıkesir), Turkey. *Ore Geology Reviews* 37, 75-101.
- Öztürk, Y.Y., Helvacı, C., Satır, M. 2005. Genetic relations between skarn mineralization and petrogenesis of the Evciler Granitoid, Kazdağ, Çanakkale, Turkey and comparison with world skarn granitoids. *Turkish Journal of Earth Science* 14, 255-280.
- Pearce, J.A., Harris, N.B.W., Tindle, A.G. 1984. Trace elements discrimination diagram for the tectonic interpretation of granitic rock. *Journal of Petrology* 25, 43-63.
- Saraç, S. 2003. Doğu Karadeniz Fe-Skarn Yataklarının karşılaştırmalı mineralojik ve jeokimyasal özellikleri. *Doktora Tezi, KTÜ Fen Bilimleri Enstitüsü*, 259s, Trabzon.
- Schultze-Westrum, H.H. 1961. Giresun Civarındaki Aksu Deresinin Jeolojik Profili, Kuzeydoğu Anadolu'da Doğu Pontus Cevher ve Mineral Bölgesinin Jeolojisi ve Maden Yatakları ile İlgili Mütalalar. *Maden Tetkik ve Arama Genel Müdürlüğü Dergisi* 57, 63-71.
- Sipahi, F. 2011. Formation of skarns at Gümüşhane (Northeastern Turkey). *Neues Jahrbuch für Mineralogy* 188, 2, 169-190.
- Sipahi, F., Akpınar, İ., Eker, Ç.S., Kaygusuz, A., Vural, A. 2017. Formation of the Eğrikar (Gümüşhane) Fe-Cu skarn type mineralization in NE Turkey: U-Pb zircon age, litho-geochemistry, mineral chemistry, fluid inclusion, and O-H-C-S isotopic compositions. *Journal of Geochemical Exploration* 182, 32-52.
- Şen, C. 1988. Dağbaşı (Trabzon) bölgesinde yüzeyleyen alt bazik (Jura)-Granitoid (Üst Kretase) formasyonlarının petrografik özellikleri. *Yüksek Lisans Tezi, KTÜ Fen Bilimleri Enstitüsü*, 92s, Trabzon.
- Yardley, B.W.D., Lloyd, G.E. 1995. Why metasomatic fronts are really metasomatic sides. *Geology* 23, 53-56.

Yılmaz, C., Kandemir, R. 2006. Sedimentary records of the extensional tectonic regime with temporal cessation: Gümüşhane Mesozoic Basin (NE Turkey). *Geologica Carpathica* 57, 1, 3-13.

Yılmaz, C., Carannante, G., Kandemir, R. 2008. The rift-related Late Cretaceous drowning of the Gümüşhane carbonate platform (NE Turkey). *Italian Journal of Geoscience* 127, 1, 37-50.

Yüksel, S. 1976. Şiran Batı yöresi Mesozoik karbonat kayaları ve eosen flisinin petrografik ve sedimantolojik incelenmesi, Doçentlik Tezi, KTÜ, Trabzon.